Optimizing nature-based solutions by combining social equity, hydro-environmental efficiency, and economic costs through a novel Gini coefficient

Cyndi Vail Castro[1]

[1]University of Houston

November 24, 2022

Abstract

A robust multi-functional decision support system for widespread planning of nature-based solutions (NBSs) must incorporate components of social equity. NBS systems advance social well-being through enhanced levels of greenspace, which have been shown to improve physical health (e.g., heart disease, diabetes), mental health (e.g., post-traumatic stress disorder, depression), and socio-economics (e.g., property values, aesthetics, recreation). However, current optimization frameworks for NBSs rely on stormwater quantity abatement and, to a lesser extent, economic costs and environmental pollutant mitigation. Therefore, the objective of this study is to explore how strategic management strategies associated with NBS planning may be improved, while considering the tripartite interactions between hydrological, environmental, and societal conditions. Here, a large-scale NBS watershed was calibrated to local conditions using standard hydro-environmental modeling (i.e., EPA's SWMM) and optimized on the basis of stormwater abatement, pollutant load reduction, and economic efficiency. The spatial allocation of possible NBS features was integrated with properties of social equity through a novel framework involving the Area Deprivation Index (ADI) and a composite Gini coefficient. By embedding social equity into the fabric of the NBS planning process, we provide an opportunity for improving social justice and spurring further community buy-in toward a balanced system. This study demonstrates how the optimal spatial placement of NBSs is location-dependent according to both the physical and human properties of the watershed.

Optimizing nature-based solutions by combining social equity, hydro-environmental efficiency, and economic costs through a novel Gini coefficient

C. V. Castro[1]

[1]University of Houston, Department of Civil and Environmental Engineering, Houston, TX.

Corresponding author: Cyndi Castro (castrocv@uh.edu)

Key Points:

- Nature-based solutions (NBSs) are traditionally planned to maximize stormwater abatement potential while minimizing implementation costs.
- Research has demonstrated the capability of NBSs to address issues of societal well-being, such as improved mental and physical health.
- A novel framework is proposed and demonstrated to combine hydro-environmental modeling with social deprivation using the Gini coefficient.

Abstract

A robust multi-functional decision support system for widespread planning of nature-based solutions (NBSs) must incorporate components of social equity. NBS systems advance social well-being through enhanced levels of greenspace, which have been shown to improve physical health (e.g., heart disease, diabetes), mental health (e.g., post-traumatic stress disorder, depression), and socio-economics (e.g., property values, aesthetics, recreation). However, current optimization frameworks for NBSs rely on stormwater quantity abatement and, to a lesser extent, economic costs and environmental pollutant mitigation. Therefore, the objective of this study is to explore how strategic management strategies associated with NBS planning may be improved, while considering the tripartite interactions between hydrological, environmental, and societal conditions. Here, a large-scale NBS watershed was calibrated to local conditions using standard hydro-environmental modeling (i.e., EPA's SWMM) and optimized on the basis of stormwater abatement, pollutant load reduction, and economic efficiency. The spatial allocation of possible NBS features was integrated with properties of social equity through a novel framework involving the Area Deprivation Index (ADI) and a composite Gini coefficient. By embedding social equity into the fabric of the NBS planning process, we provide an opportunity for improving social justice and spurring further community buy-in toward a balanced system. This study demonstrates how the optimal spatial placement of NBSs is location-dependent according to both the physical and human properties of the watershed.

1 Introduction

Nature-based solutions (NBS) describe a collection of sustainable management approaches that emulate natural processes to address hydro-environmental hazards while simultaneously providing social and ecosystem benefits. NBSs have evolved within the literature to encompass the urban drainage concepts of green infrastructure (GI), low-impact development (LID), best management practices (BMPs), sustainable urban drainage systems (SuDs), water-sensitive urban design (WSUD), and blue-green infrastructure (BGI) (Ruangpan et al., 2020). As such, the predominant modeling schemes used for NBS planning have typically highlighted hydrological efficiency with less attention to social characteristics (K. Zhang & Chui, 2018). However, we know that the location of human settlements can influence several social factors that have been linked to NBS co-benefits, such as improvements in communal well-being, mental health, recreation, and physical health (Alves et al., 2019; Fenner, 2017; Li et al., 2017). By providing enhanced greenspaces and social gathering places, NBSs have been linked to a reduction in cardiovascular disease, diabetes, cancer, mental disorders, and chronic respiratory diseases, which are disproportionately higher among racial and ethnic minorities and the socioeconomically disadvantaged (Astell-Burt & Feng, 2021; Brown et al., 2016; Fuertes et al., 2014; Gascon et al., 2016; Maas et al., 2009; Mitchell & Popham, 2008; Ray & Jakubec, 2014). As such, we must integrate hydro-environmental and social characteristics to realize the full benefits of NBSs.

At the local scale (i.e., laboratory-, plot-, neighborhood-scale), NBS technologies have shown great promise in addressing both stormwater abatement goals and socio-environmental co-benefits (Jato-Espino et al., 2016; Kabisch et al., 2016; Loperfido et al., 2014). At the regional scale, however, widespread use of NBS technologies has been limited due to a lack of understanding the complex interactions between physical characteristics and social conditions (Lim & Welty, 2017; K. Zhang & Chui, 2018). When planning for NBS systems, there will exist inherent tradeoffs between spatial priority and functionality that must be considered. The optimal spatial configuration of an NBS system is a function of overlapping rainfall patterns, watershed properties, equity factors, environmental triggers, ecological considerations, socio-demographics, risk and vulnerability, and other underlying principles that have not been fully elucidated (Perez-Pedini et al., 2005). Traditionally, NBS optimization schemes have continued to prioritize drainage characteristics in lieu of social functionality throughout space, while assuming such co-benefits will somehow propagate naturally throughout the system (Ruangpan et al., 2020; K. Zhang &

Chui, 2018). In this way, NBS multi-functionalities are not included as an explicit representation of their full locational benefits, thus limiting the maximum potential of NBSs to mitigate cross-cutting issues within the urban fabric. A right first step toward fully encompassing NBS multi-functionalities is to represent disparate phenomena as functions of space and to quantify their tradeoffs through the lens of overlapping disciplines.

In the age of the Anthropocene, where hydrologic, environmental, and social processes are being influenced and altered by human patterns, we are starting to study Earth systems outside of the traditionally-fixed vacuum of ideal physical boundary conditions. Researchers are beginning to couple biophysical processes with societal influences through the flourishing fields of socio-hydrology, coupled human and natural systems (CHANS), socio-ecology, and others (Blair & Buytaert, 2016). The hydrological community is suggesting that we address socio-environmental justices by integrating transdisciplinary variables into watershed modeling frameworks. Much of the recent progress in socio-hydrology has evolved from a combination of exploratory frameworks (i.e. feedbacks, causal relationships, patterns) with water balance models and system dynamics (Kuil et al., 2016; Pande & Sivapalan, 2017). While such couplings have been widely noted within the literature, they are seldom quantitated and considered holistically in NBS management frameworks (Ruangpan et al., 2020).

NBS systems are instead typically planned with either simplified data-overlay methods for defining hot-spots of vulnerable locations or complex hydro-dynamic programs that prioritize stormwater volume abatement over social functionalities (Madureira & Andresen, 2014; K. Zhang & Chui, 2018), with the latter being limited in their scale of analysis due to large data requirements and computational difficulties (Barco et al., 2009). By relying on complex modeling tools (i.e., SWMM, MIKE-URBAN), most NBS studies have tended to neglect the social dimension altogether in favor of earth-system processes, thereby lacking optimal configurations for capturing holistic co-benefits (Kandakoglu et al., 2019). For these reasons, widespread adoption of green infrastructure has generally remained stunted, despite the ongoing evidence that NBSs provide efficient stormwater mitigation, lower costs in comparison to traditional grey infrastructure, and numerous social benefits (Golden & Hoghooghi, 2018; Madureira & Andresen, 2014). A recent state-of-the-art review described how consideration of multiple co-benefits has been increasingly valued as a desirable goal throughout the NBS literature, yet the majority of NBS planning has continued to prioritize stormwater abatement, due in part to a lack of integrated socio-hydrological

frameworks (Ruangpan et al., 2020). We thereby have substantial knowledge gaps regarding informed NBS optimization (Golden & Hoghooghi, 2018; Kabisch et al., 2016), as interactions between NBS phenomena and the social conditions with which they aim to address are poorly represented in our existing frameworks (Lim & Welty, 2017). As such, explicit representation of the social co-benefits of NBS systems is one of the most critical barriers to overcome for widespread success in this field (Adib & Wu, 2020).

In addition to a lack of robust representation of social characteristics within NBS optimization frameworks, the decision to implement NBS within a given locale is also highly dependent on stakeholder buy-in (Van de Meene et al., 2011; Wihlborg et al., 2019). NBSs are unlike traditional stormwater infrastructure due to regular human interaction with greenspace, which impacts social well-being. Many NBS technologies, such as roof gardens or rainwater harvesting systems, function as an optimal unit when implementation occurs on both public and private properties. In this respect, local community buy-in is essential for achieving widespread NBS adoption. Studies have demonstrated how NBS implementation continues to be limited due to the inability for decision-makers to visualize overlapping co-benefits at the local scale (Adib & Wu, 2020; L. Liu & Jensen, 2018; Van de Meene et al., 2011; S. E. Sarabi et al., 2019; Wamsler et al., 2020; Wihlborg et al., 2019). Studies have also shown that attitudes regarding NBSs are improved when stakeholders can readily identify how NBS solutions will benefit their locale in a manner that extends beyond stormwater performance (L. Liu & Jensen, 2018; S. Sarabi et al., 2020; Wamsler et al., 2020). In other words, robust NBS implementation will not occur until city planners are able to identify and prioritize the multiple co-benefits involved in the NBS system. As such, in order to fully capture the multi-functionalities of NBS systems and improve implementation, we necessitate innovative optimization frameworks encompassing the variety of physical and social functionalities associated with NBSs.

Current stormwater management within the study area (Houston, Texas, USA) is based on a ‘worst-first’ framework (Despart, 2019), where hydrological improvements are prioritized according to flood risk reduction and the number of persons benefited, irrespective of their socio-economic conditions. Such frameworks do not address inherent vulnerabilities within the populations served to consider human aspects, such as ability to recover from a storm or the reinforcing impacts of hydro-environmental hazards on socio-economics. This study re-shapes the NBS planning process by transcending beyond flood risk to also include components of social

characteristics as a policy-making mechanism. Here, a novel equity-based indexing framework is proposed to better understand how we might optimize social and physical functionalities of NBS systems as a function of trans-disciplinary characteristics. Specifically, this study explores the spatial tradeoffs associated with NBS allocation by first optimizing a local watershed-scale model according to traditional metrics of efficiency (e.g., cost efficiency, hydrological runoff reduction, and pollutant load reduction). The statistical dispersion of social vulnerability is then identified using the Area Deprivation Index (ADI), which is a spatial account of neighborhood disadvantage according to United States census characteristics. The ADI is incorporated into the optimization scheme using a novel area Gini coefficient and Lorenz curve. This framework is intended to spur the positive connection of social and physical influences within robust NBS planning.

2 Materials and Methods

2.1 Area Deprivation Index

The ADI was introduced in 2016 as a proxy indicator of socio-economic status from census results that have been curated to reflect the highest risk factors associated with long-term health (Knighton et al., 2016). The ADI is primarily used within the medical literature to measure social determinants that have been shown to influence public health issues, such as cancer rates (Kurani et al., 2020), hospital admissions (Hirshberg et al., 2019; Ingraham et al., 2021), asthma (Nkoy et al., 2018), obesity (Ludwig et al., 2011), diabetes (Addala et al., 2021), mental health (Martikainen et al., 2004), and mortality (Chamberlain et al., 2020; Singh, 2003), each of which are impacted by NBS systems (van den Bosch & Ode Sang, 2017). The ADI merges characteristics of income, employment, education, and housing from the United States census to represent social disadvantage (Kind & Buckingham, 2018), which have been shown collectively to influence communal health (Link & Phelan, 1995).

An advantage of using the ADI for NBS planning, as opposed to other social indices, involves its highly-granular geospatial scale. The ADI provides a unique measurement of social deprivation for each census block group within the United States. Other standard metrics of social vulnerability, such as the Center for Disease Control (CDC) Social Vulnerability Index (SVI) (Flanagan et al., 2020), are delineated at the census tract-scale, thereby lacking spatial heterogeneity to assess key differences between neighborhoods. [Note: Census tracts are subdivisions of counties encompassing approximately 4,000 residents within each bound. Block

groups are subdivisions of census tracts encompassing approximately 250-550 housing units, demarcated by local streets (Schlossberg, 2003).]

The ADI for the study area was downloaded from the University of Wisconsin's Neighborhood Atlas for year 2019 (Kind & Buckingham, 2018). The weighted ADI values within each spatial unit are represented at the national-level by a percentile (1-100) and at the state-level by a decile (1-10), with lower values denoting greater disadvantage (University of Wisconsin School of Medicine and Public, 2019). For example, an ADI value of 1 on the national-scale represents an area that is more disadvantaged than the remaining 99% of census blocks within the nation. At the state-scale, an ADI of 1 implies that the given census block is more disadvantaged than 90% of the other census blocks within that state.

Here, the national-level ADI was used to depict spatial variation of social inequity throughout the White Oak Bayou (WOB) watershed in Houston, Texas, USA. The WOB watershed was chosen for this case study as it contains a highly-heterogeneous representation of socio-economic status.

2.2 Hydro-environmental SWMM Model

2.2.1 Hydrological Modeling

The basin model for the WOB watershed was initialized using the HMS-PrePro tool, which rapidly delineates a watershed into subcatchments according to the local terrain, connects hydrological topology in a format consistent with standard hydrological modeling software, and estimates common hydrological parameters to represent basin infiltration, runoff, and channelized routing of flow (Castro & Maidment, 2020). The Green-Ampt method was used to represent infiltration losses within each subcatchment according to local empirical values used in FEMA-effective hydrology models for the WOB watershed (HCFCD, 2019) (initial content = 0.067, saturated content = 0.46, suction = 3.553 inches, conductivity = 0.032 inches/hour). The SWMM software routes overland flow to the subcatchment outlet using a property called the "characteristic width," which is defined as the subcatchment area divided by the average maximum overland flow length (L. A. Rossman & Huber, 2016). The longest flow path for each subcatchment was calculated in HMS-PrePro according to 2018 LiDAR at 10-centimeter resolution (TNRIS, 2019). The time of concentration for each subcatchment was calculated using the TR-55 methodology for

urban watersheds (USDA, 1986).Other principal inputs for modeling subcatchments in SWMM include average land use, impervious coverage, subcatchment area, and terrain slope, which were each estimated using HMS-PrePro.

PCSWMM version 7.4.3240 (Hamouz et al., 2020), which is a proprietary software designed as a user-friendly interface to the Environmental Protection Agency (EPA) SWMM program, was used to convert the basin into a SWMM model. To route flow through the watershed stream network, the PCSWMM Transect Tool was used to create average cross-sections for each system channel from the 2018 LiDAR elevation model (CHI, 2014). Design storm data for the Houston region was obtained from Barrett (2019) and COH (2019) to represent the latest precipitation frequency estimates in Texas, according to the National Oceanic and Atmospheric Administration (NOAA) Atlas 14 (Perica et al., 2018). The rainfall intensity values for the Houston-area were used to develop intensity-duration-frequency (IDF) curves in PCSWMM for varying annual exceedance probability (AEP) storm events (summarized in **Table S.1**). The IDF curve estimates a frequency of occurrence for extreme precipitation events, which is commonly used to design urban stormwater infrastructure (Koutsoyiannis et al., 1998).

2.2.2 Pollutant Load Modeling

The event mean concentration (EMC) method was used to estimate non-point water pollution within each subcatchment according to

$$EMC_s = \frac{\int C_s Q_s \, dt}{\int Q_s \, dt}, \tag{1}$$

where EMC_s is the event mean concentration, C_s is the standard concentration of a target pollutant, and Q_s is the runoff volume for each subcatchment, s, changing over simulation time, t.

Local stormwater monitoring data was obtained from the National Stormwater Quality Database (NSQD), which contains public water quality meta-data from over 9,000 runoff events for approximately 200 municipalities in the United States, including 41 monitoring stations within Harris County, Texas (Pitt et al., 2015). Since the GreenPlan-IT algorithm searches for the most cost-effective solution according to an individual pollutant type (further described in **Section 2.3**), total suspended solids (TSS) were chosen as the criteria pollutant due to the strong adsorption effects of TSS on other contaminants (Yang Liu et al., 2019; Rossi et al., 2006). Pooled values of TSS concentrations were obtained for each land use type within the NSQD, as summarized in

215 **Error! Reference source not found.**. In watershed-scale modeling, pooled load concentrations
216 are commonly used and have not been shown to pose a significant impact on the resulting model
217 outcomes, particularly when the purpose of analysis is for comparison between scenarios (Lin,
218 2004; M. White et al., 2015).

219 The land use values in the WOB basin model were obtained from the 2016 National Land
220 Cover Database (NLCD), which contains 16 unique land classifications based on the modified
221 Anderson Level II scheme (Yang et al., 2018). The NLCD land uses were re-classified to
222 correspond with the five land use types used in the NSQD, as shown in **Error! Reference source**
223 **not found.**. The removal efficiency for each of the NBS types modeled in this study were obtained
224 from the 2020 International Stormwater BMP Database (Clary et al., 2020), which corresponds
225 well with average removal efficiencies in the NBS literature for watershed-scale NBS modeling
226 (e.g., Eckart et al. (2017); Liu et al. (2015)).

227 *2.2.3 NBS Water Balance Modeling*

228 EPA's SWMM engine calculates the water balance for NBS-driven systems using a
229 nonlinear reservoir model (Chen & Shubinski, 1971) according to a unique set of infiltration,
230 storage, and evaporation properties that describe, on a per-unit-area basis, how NBS structures
231 impact hydrological behavior. A subset of zones and water fluxes as a function of NBS behavior
232 is depicted in **Figure 1** (L. A. Rossman & Huber, 2016).

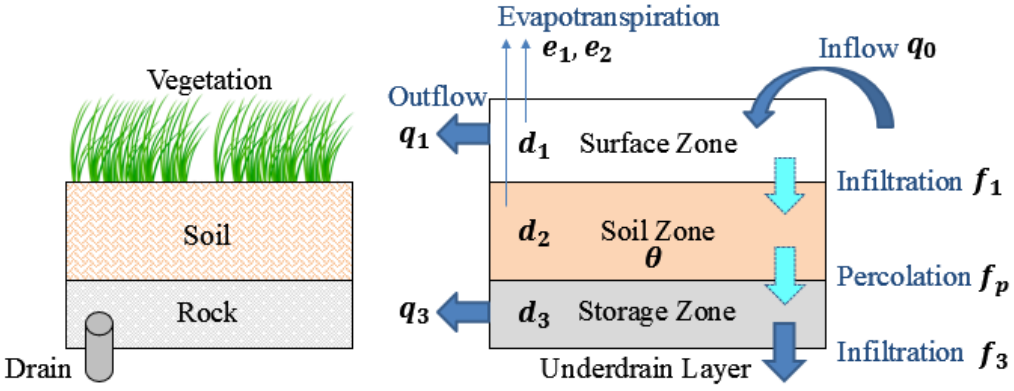

233

234 **Figure 1.** Conceptual model of NBS water balance processes.

235 The water fluxes are defined by:

236 $$\frac{\partial d_1}{\partial t} = q_0 - e_1 - f_1 - q_1, \quad (2)$$

$$d_2 \frac{\partial \theta}{\partial t} = f_1 - e_2 - f_{\mathrm{p}}, \quad (3)$$

and

$$\frac{\partial d_3}{\partial t} = f_{\mathrm{p}} - f_3 - q_3, \quad (4)$$

where d_1 is the depth of ponded water on the surface zone with outflow q_1 (cfs), d_2 is the depth of the soil zone with moisture content θ, d_3 is the depth of the storage zone with outflow q_3 (cfs), q_0 describes the inflow to each NBS cell (cfs), e_1 and e_2 represent the evapotranspiration from the surface zone and the soil zone, respectively, f_1 describes infiltration between the surface and soil zone, f_{p} is percolation between the soil and storage zone, and f_3 is infiltration from the storage zone to the underdrain layer.

The flux terms (q, e, f) are functions of the water content within each layer and subcatchment site conditions. The set of equations is solved at each runoff time step, according to the Green-Ampt method, to calculate how the inflow hydrograph to the NBS unit is converted to a runoff hydrograph, further described by Rossman (2014).

Within NBS systems, the surface zone represents the ground surface, which stores excess inflow and generates outflow either overland or to an adjacent drainage system. The soil zone is comprised of an engineered soil mixture that allows water to percolate into the underlying zone, which consists of rock and gravel for additional storage. The underdrain system conveys water out of the storage layer and into an engineered outlet. The three NBS features used in this case study (bioretention cells, porous pavement, and tree boxes) are described in Error! Reference source not found. as a function of the representative water balance layers modeled in PCSWMM. In the WOB case study, tree boxes were modeled as bioretention cells with no outflow drain.

Various input parameters are also required within a SWMM model to describe the engineered design of local NBS features (e.g., conductivity rate, vegetation volume, clogging properties, surface roughness, etc.), which were obtained from the City of Houston design guidelines for low impact development (COH, 2019a), as summarized in **Table S.4**.

2.2.4 Calibration & Validation

The hydrological basin parameters were calibrated to observed streamflow measurements from United States Geological Survey (USGS) stream gauges #08074020 and #08074500 (USGS,

2021a, 2021b). One year of daily precipitation values were obtained from the Harris County Flood Warning System (HCFWS) precipitation gauges #530, #535, #550, #555, #560, #570, #582, #590, and #595 (HCFCD, 2021), encompassing the totality of the White Oak Bayou watershed. The first six-months of precipitation data (October 2, 2020 – March 2, 2021) were used to calibrate the model, while the latter six-months of data (March 3, 2021 – August 2, 2021) were used to validate the model. The PCSWMM sensitivity-based radio tuning calibration (SRTC) tool was used to aid in identifying the most sensitive parameters within the model, according to user-identified uncertainty, and for calibrating the model to match observed streamflow (CHI, 2015). The annual set of hydrographs for the basin model was disaggregated for wet weather conditions with a criterion of at least 500 cfs flow for a minimum of 4 consecutive hours, resulting in ten unique storm events for calibration and eight unique storm events for validation. The wet weather flow hydrographs were calibrated using the PCSWMM SRTC tool by selecting uncertainties for control parameters based on their data source and sensitivity gradient, per guidelines proposed by Choi and Ball (2002) and James (2003). The basin model was then simulated with the calibrated parameters and compared to observed streamflow and resulting error metrics to measure goodness-of-fit.

The error metric employed in this study was the integrate square error (ISE), which amalgamates differences between observed and calibrated values according to overall storm runoff volume, peak flow, mean flow, and the hydrograph time to peak (James, 2003). The ISE is advantageous over the traditional Nash-Sutcliffe efficiency (NSE) or coefficient of determination (R^2) because these latter error metrics are both sensitive to outliers and tend to converge on one measure of hydrological efficiency (i.e., total runoff or peak flow or average runoff) (CHI, 2020). The ISE is recommended for large-scale watershed planning due to its capability to assess goodness-of-fit over a range of historical rain events and hydrograph parameters, rather than potentially biasing the model to one specific event or metric of performance (CHI, 2015). Moreover, the ISE is beneficial in urban watersheds that are modeled without sub-surface flow because sewer system hydraulics may be indirectly calibrated using the ISE, whereas the NSE is dominated solely by overland flow conditions (Sarma et al., 1973).

The ISE is expressed as

$$ISE = \frac{\sqrt{\sum\left(y_{obs}^{i} - y_{comp}^{i}\right)^{2}}}{\sum y_{obs}^{i}}, \quad (5)$$

where y_{obs}^{i} is the observed value, and y_{comp}^{i} is the computed value for the i-th observation. Then, the rating of the resulting ISE error metric may be defined on a qualitative scale, as defined by Sarma et al. (1973), such that ISE ≤ 3 = Excellent, 3 < ISE ≤ 6 = Very Good, 6 < ISE ≤ 10 = Good, 10 < ISE ≤ 25 = Fair, and ISE > 25 = Poor.

The model calibration and validation hydrographs and ISE error metrics are demonstrated in supplementary materials (**Figure S.1 – Figure S.3** and **Table S.5 – Table S.6**), respectively.

2.3 Spatial Allocation Optimization

A decision support tool, called GreenPlan-IT, was used to optimize the fully-calibrated watershed model according to levels of runoff reduction, pollutant load abatement, and cost effectiveness (Wu et al., 2019) (see **Figure 2a-b**). GreenPlan-IT couples the nondominated sorting genetic algorithm (NSGA-II) with the EPA SWMM software according to the Pareto front solution (SFEI, 2018). The GreenPlan-IT package combines several unique tools that operate in succession to identify the optimal spatial allocation of NBS features, including:

1. GIS-based Site Locator Tool (SLT): Merges spatial characteristics of NBS types with regional geospatial information to identify all possible NBS locations within the study area.

2. EPA SWMM Basin Model: Establishes baseline conditions for runoff and pollutant loading prior to NBS optimization.

3. GreenPlan-IT Optimization Tool (GPOT): An executable file that runs through the user's command prompt to identify optimal combinations of NBS types within each catchment area according to a cost-benefit analysis (where costs are defined by the user, and benefits are calculated using SWMM to assess the reduction in stormwater runoff and pollutant loads for many simulations).

The GIS-based SLT was used to identify all potential locations of NBS features within the WOB watershed. Potential locations for bioretention cells, permeable pavement, and tree boxes were defined according to open space land use parcels, areas of existing pavement, and adjacent land near existing sidewalks, respectively. Corresponding data layers were obtained from the City of Houston GIS Data Hub (COH, 2021).

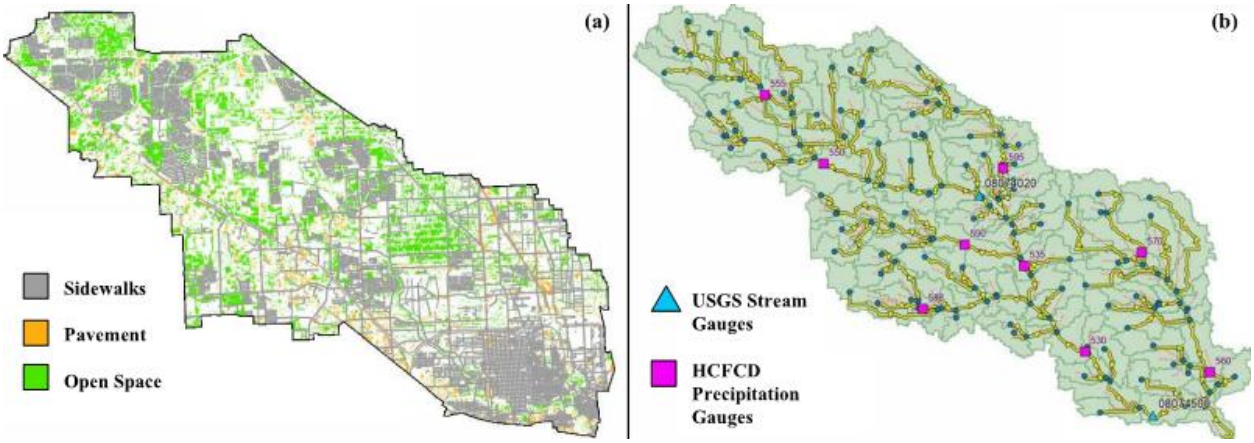

Figure 2. (a) Geospatial siting of potential NBS locations in the WOB watershed; **(b)** PCSWMM basin model, stream gauges, and precipitation gauges for WOB.

Baseline flow and TSS loads were quantified within the SWMM model for various design storm events, as described in **Section 2.2**. The SLT output then served as a spatial constraint for the GreenPlan-IT Optimization Tool, which executes several hundred SWMM models according to unique spatial allocations of NBS features within the permissible areas (i.e., the shaded areas shown in **Figure 2a**). The GPOT compares the performance of various NBS strategies to the baseline scenario, which represents watershed conditions prior to NBS implementation. Model performance is defined by three objectives: 1) minimized total relative cost of NBS implementation, 2) maximized reduction in hydrological runoff, and 3) maximized abatement of pollutant loads within the study area.

Relative cost estimates for the case study were obtained from the EPA National Stormwater Calculator (NSWC), which provides annual costs for NBS implementation and maintenance within unique geographical regions. At the time of study, the NSWC cost estimates for the Houston-area included: pervious pavement = $8.68/SF, bioretention cells = $6.07/SF, and tree planter boxes = $9.46/SF (Bernagros et al., 2021). The GPOT uses two input files to compare NBS scenarios with the baseline SWMM model. The first input file contains the total acreage and percent impervious coverage for each subcatchment and the maximum number of possible NBS sites per subcatchment from the GIS-based SLT, as summarized in **Table S.7**. The second input file describes sizing parameters, where the NBS features were assigned a uniform unit area and width of 500 SF by 20 FT, 5000 SF by 50 FT, and 60 SF by 6 FT for bioretention cells, pervious pavements, and treeboxes, respectively.

346 The NSGA-II algorithm, originally presented by (Deb et al., 2002), searches for the optimal
347 solution among numerous possible scenarios by first modeling a random set of NBS placements
348 and comparing their outputs for non-dominance. Non-dominance occurs when a solution performs
349 no worse than any other solution for all objectives (e.g., cost, runoff, and pollutant load efficiency)
350 and also performs better than all other solutions within the cohort for at least one objective. This
351 cohort (known as a generation), then sorts each of the sub-routines within the series (known as
352 populations) for non-dominance. Another generation is run using the previous generation's non-
353 dominant solutions and relative population samples. This iteration continues until the system either
354 reaches a maximum number of generations or until no further changes are observed between two
355 consecutive populations. The primary GreenPlan-IT tool, which was designed for use in the greater
356 San Francisco Bay area, uses a threshold of 200 generations, each with a population size of 100,
357 for a maximum of 20,000 watershed simulations (SFEI, 2018). The GreenPlan-IT tool was
358 modified in concert with the tool developers for use in Houston, Texas, which resulted in an
359 NSGA-II stop criteria of 100 generations, each with a population size of 250 model runs. As a
360 result of this collaboration, it is our understanding that future versions of GreenPlan-IT will be
361 released to allow application in other large watersheds, such as the WOB. The model outputs of
362 the optimization tool are plotted as a function of cost (x-axis) versus runoff or load reduction (y-
363 axis), resulting in a Pareto curve (see **Section 3.1**). Each point along the convex of the Pareto curve
364 (known as the Pareto front) represents a unique, quasi-optimal solution for NBS spatial allocation
365 according to the cost and reduction targets located on the curve axes (Wu et al., 2019).

366 **2.4 Multi-objective Gini Index**

367 The Gini coefficient, which was originally identified by Gini (1912), is a statistical
368 representation of inequality across a population. The Gini coefficient is based on the Lorenz curve,
369 depicted in **Figure 3**, which describes the cumulative proportion of values along the x-axis
370 compared with the cumulative proportion of values along the y-axis. Within the social sciences,
371 the Gini-based approach is commonly used to assess the degree of matching between population
372 (x-axis) and income/wealth (y-axis) for economic purposes to quickly compare and rank disparate
373 geographic entities (Giorgi & Gigliarano, 2017).

374 In a perfectly-equal scenario, the distribution of income matches the distribution of the
375 population, shown as the diagonal line in **Figure 3**. In a more realistic scenario, the normalized

376 percentage of population to percentage of household income typically follows an exponential
377 distribution, known as the Lorenz curve, which delineates state spaces **A** (e.g., the inequality gap)
378 and **B** (e.g., the actual income distribution) in **Figure 3**.

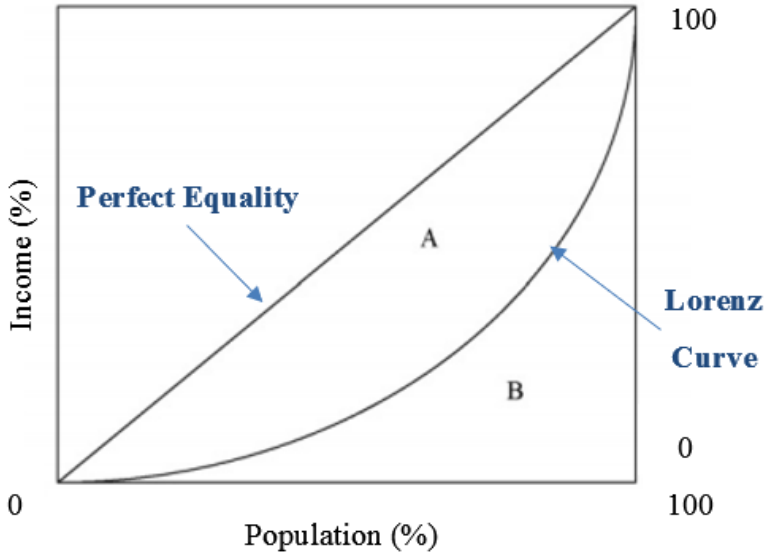

379
380 **Figure 3.** Conceptual graph of Gini-based equality and Lorenz curve.

381

382 The Gini coefficient (G) is expressed graphically by

383 $$G = \frac{A}{(A+B)}, \tag{6}$$

384 where A represents the total area between the line of equality and the Lorenz curve distribution,
385 and B represents the area between the Lorenz curve and the base axes.

386 A numerical form of the Gini coefficient (G_i) is given by

387 $$G_i = 1 - \sum_{i=1}^{n} (Y_i - Y_{i-1})(X_i + X_{i-1}), \tag{7}$$

388 where X_i is the cumulative percentage of the variable on the x-axis, and Y_i is the cumulative
389 percentage of the variable on the y-axis, for data point i, from i=1 to i= n total data points.

390 Gini coefficient values range from 0 to 1, where 0 indicates absolute equality, and 1
391 represents absolute inequality. Due to the popularity of the Gini coefficient to quickly identify
392 statistical differences in equality, studies have begun applying this economic concept to issues of
393 energy allocation (Jacobson et al., 2005; Saboohi, 2001), environmental inequity (Boyce et al.,
394 2016; Heerink et al., 2001; T. J. White, 2007), water resources allocation (Cho & Lee, 2014; Du

et al., 2021; Hu et al., 2016; Yan et al., 2018), flood drainage rights (D. Zhang et al., 2020), and other topics regarding distribution of limited resources (Josa & Aguado, 2020).

Many of the recent applications of the Gini concept to issues of environmental concern utilize the area-based Gini coefficient. The area-based Gini ("AR-Gini") compares a social metric, calculated on an area basis, to a distributed social good, calculated on a resource basis (Druckman & Jackson, 2008). The AR-Gini may be used to compare spatial patterns of space-based resources and population-based social metrics to reveal internal relationships, improve planning frameworks, and identify useful cross-disciplinary spatial indicators. An example of using the AR-Gini coefficient beyond the traditional scope of economic wealth disparity is given by Sun et al. (2010) where wastewater discharge permitting is optimized using the Gini index and a multi-criteria assessment of land, population, income, and environmental capacity. In the AR-Gini study, the conflict between wastewater efficiency and social equality is bridged by balancing tradeoffs between various policy-making goals amidst limited resources (Sun et al., 2010).

The method presented here uses a novel representation of the AR-Gini to advance sustainability planning by combining hydrological, environmental, and social efficiencies within NBS spatial allocation optimization. The cumulative area of NBS allocation as a proportion of each subcatchment area is plotted on the y-axis, normalized on a scale from 0-100. Unique evaluation indicators (i.e., stormwater runoff, stormwater quality, and social equity) are then plotted on the x-axis, such that each potential optimization model contains three different Gini coefficients. Hydrological efficiency is represented as the percent difference of stormwater runoff volume between baseline and optimized conditions as a function of cost. Environmental efficiency is described as the percent difference of pollutant load abatement between baseline and optimized conditions according to cost. Social equity is a function of the average neighborhood disadvantage over the weighted area of NBS allocation within each subcatchment. By minimizing the sum of these multi-objective Gini coefficients, this novel approach reveals the state space of optimal hydrological efficiency and distribution of NBSs in socially-vulnerable locations.

Minimizing the Gini coefficient as a function of hydrological efficiency and social justice provides the novel framework for allocating NBSs according to both their hydrological functionality and also the social characteristics of persons that would be influenced by varying spatial arrangements. A high Gini coefficient would reveal that the distribution of NBSs using only

hydrological efficiency does not maximize the multi-functional goals of improving societal health through improved access to nature. To my knowledge, this is the first attempt to utilize the Gini coefficient for optimizing allocation of NBSs according to combined social equity and hydro-environmental efficiency. Here, several of the SWMM-based optimization scenarios from the GreenPlan-IT tool are calculated using the multi-functional Gini calculations, described below, to better understand the trade-offs between hydro-environmental/economic efficiency and spatial equality when planning watershed-scale NBS solutions. The first objective is to maximize the economic benefit efficiency of hydro-environmental spatial optimization. The second objective is to maximize social equity using a composite AR-Gini coefficient. In doing so, a hypothesis is generated from robust hydro-dynamic modeling, which is then tested against the spatial representation of social deprivation to elicit a numerical hypothesis of holistic NBS conditions that are optimally distributed to maximize urban greening in areas of highest social vulnerability. The following equations are applied in deriving the multi-objective Gini coefficient:

$$\omega_s = \sum_{j=1}^{n} z_{js} A_j \,, \tag{8}$$

where ω_s is the allocation of NBS area per subcatchment s, n is number of unique NBS feature types j = bioretention cells, porous pavements, or tree boxes, z is the number NBSs per subcatchment, A_j is the area of each NBS feature type (A_j: bioretention cells = 500 SF, porous pavements = 5,000 SF, tree boxes = 60 SF),

$$\eta_s = \frac{\left(\frac{a_s - b_s}{a_s}\right) * 100}{\sum_{j=1}^{n} z_{js} A_j c_j}, \tag{9}$$

where η_s is the percent efficiency of hydro-environmental improvement between the baseline model, a, and the optimized model, b for each subcatchment s as a function of the cost for each NBS feature, c_j (c_j = \$6.07/SF, \$8.68/SF, \$9.46/SF for j=bioretention cells, porous pavements, and tree boxes, respective); a and b represent the total stormwater runoff volume (VR, in million gallons) for hydrologic efficiency and the total pollutant load runoff (TSS, in lbs) for environmental efficiency, from SWMM modeling.

$$\mu_s = \frac{ADI_s}{\sum_{s=1}^{m} \omega_s}, \tag{10}$$

where μ_s is the percent of social inequality addressed by the optimized model according to the total NBS allocated area within each subcatchment, ω_s, for all subcatchments m, and the social

inequality within the subcatchment is measured by the average spatial Area Deprivation Index (ADI) score within each subcatchment ADI_s.

To eliminate differences in measurement units and magnitudes among evaluation choices, each indicator is then normalized on a scale of 0 to 100 per

$$\tilde{x} = \frac{x - x_{min}}{x_{max} - x_{min}}, \tag{11}$$

where $\tilde{x}$ is the normalized value of each x = hydrologic efficiency (η_s), environmental efficiency (η_s), and social equity (μ_s).

Consequently, the sum of the normalization series for each Lorenz curve axis is 100. The Gini coefficient is then calculated by:

$$Y_s = Y_{s-1} + \frac{\widetilde{\omega_s}}{\sum_{s=1}^{m} A_s} * 100, \tag{12}$$

$$X_s = X_{s-1} + \left(\frac{\widetilde{\eta_s}}{\sum_{s=1}^{m} \widetilde{\eta_s}} \middle| \frac{\widetilde{\mu_s}}{\sum_{s=1}^{m} \widetilde{\mu_s}} \right) * 100, \tag{13}$$

$$G_i = 1 - \sum_{s=0}^{m} \left(X_s - X_{(s-1)}\right)\left(Y_s - Y_{(s-1)}\right), \tag{14}$$

where Y_s is the y-axis value on the Lorenz curve, X_s is the x-axis value on the Lorenz curve, A_s is the area of each subcatchment s, with total subcatchments m, and G_i is the Gini coefficient corresponding to the evaluation index i = runoff volume efficiency, pollutant load efficiency, or social equity distribution. X_s and Y_s are plotted on the Lorenz curve by sorting Y_s in ascending order, where X_0 and Y_0 each equal 0.

Finally, the composite optimization objective is represented by

$$Optimization\ Objective: min \sum_{i=1}^{3} G_i, \tag{15}$$

where G_i is the multi-functional Gini coefficient for each indicator, i.

In summary, the following steps are applied to calculate the composite Gini index for amalgamating a series of NBS efficiency indicators according to both social deprivation and hydro-environmental risk:

1. Select a set of potential NBS allocation scenarios according to hydro-environmental SWMM-based optimization modeling,
2. Calculate Lorenz curve values for each efficiency indicator (hydrologic, environmental, and social) and NBS scenario according to **Eq. 9-14**,

3. Plot the Lorenz curves and calculate each G_i using **Eq. 7** and/or **Eq. 15**,
4. Aggregate the objective functions and compare Lorenz curves according to the multi-criteria Gini coefficient, **Eq. 16**,
5. Identify the greatest distribution of social equality and hydro-environmental efficiency by minimizing the objective function in **Eq. 16**.

3 Results & Discussion

3.1 Hydro-environmental Pareto Front Curve

The GreenPlan-IT optimization tool for the WOB watershed converged after 100 generations (i.e., series), each with approximately 250 population values per generation. The 2-, 5-, and 100-year rainfall events were chosen as representative design storms for demonstrating the hydro-environmental optimization results, as demonstrated in **Figure 4**. An example of planning for NBS expenditure of $1,000M is shown in the dashed lines where the optimal Pareto front results in a flow reduction of 3.22%, 3.62%, and 4.37% and a TSS pollutant load reduction 11.69%, 11.65%, and 9.55% of for the 2-, 5-, and 100-year design storms, respectively. The cost-effectiveness curves (i.e., the Pareto fronts) suggest there exists a largely linear relationship between the level of NBS implementation and TSS pollutant load reduction between the 2-year and 5-year design storms. Decision-makers can then use these results to determine optimal NBS planning according to target expenditures. The cost-effectiveness curve in **Figure 4** informs which Generation and Population model provides the most efficient hydro-environmental outcomes from the ~25,000 scenarios that were simulated in SWMM. By assessing the far-right portion of the Pareto front, decision-makers may identify at which point further investment in NBS technologies yield no additional improvement in hydro-environmental goals.

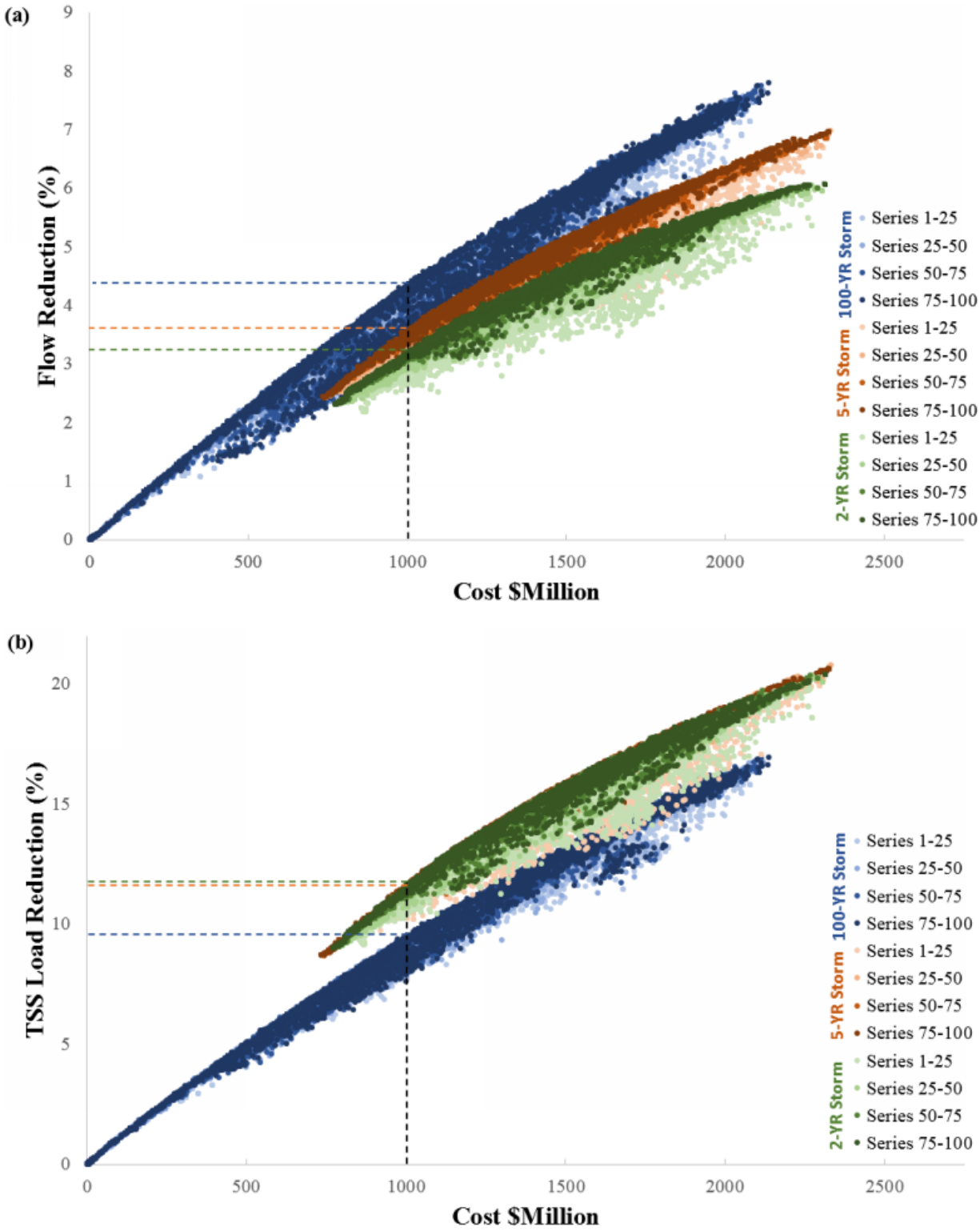

Figure 4. GreenPlan-IT optimization output for WOB: **(a)** flow reduction as a function of cost-efficiency; **(b)** pollutant load reduction as a function of cost-efficiency.

As such, hydrologic versus environmental efficiency goals may be compared and contrasted between scenarios as a function of cost distribution and intensity of design storm metrics (SFEI, 2020). For example, if decision-makers had a goal of reducing the 100-YR storm flow by 5% (equating to a total cost of $1,187M on the hydrologic cost-effectiveness curve), stakeholders could quickly visualize the flow reduction efficiency for additional design storms and the tradeoffs associated with pollutant load abatement at this cost point. To demonstrate how such optimization outputs may be combined with the multi-objective Gini coefficient described in **Section 2.4**, the 5-YR storm event with $1,000M NBS expenditure was chosen for further analysis. In this scenario, Generation 97, Population 117 produced the most optimal NBS allocation scenario according to hydro-environmental efficiency. In comparing the spatial distribution of NBSs from this model with the areas of highest social deprivation in the WOB watershed (reference **Figurea-b**), we may note how sole reliance upon hydrological characteristics for NBS planning could result in a missed opportunity to address potential social benefits from enhanced urban greening. As such, the multi-objective Gini is explored to further refine the NBS optimization results.

3.2 Gini-based Optimization

A Gini coefficient less than or equal to 0.4 is commonly used as a threshold denoting fair distribution between the indicators on the x- and y-axes of the Lorenz curve (Groves-Kirkby et al., 2009; Sadras & Bongiovanni, 2004). By plotting the Lorenz curves for the SWMM-based optimization model (Generation 97, Population 117) in **Figure 5**, the Gini coefficients according to hydrologic efficiency, pollutant load efficiency, and social equity were calculate as 0.17, 0.10, and 0.46, respectively. Such results suggest a greater equity in NBS allocation on the basis of hydro-dynamics compared with social characteristics. The large area between the Lorenz curve arc and the line of equality in **Figure 5c** reveals poor allocation fairness corresponding to spatial distribution of neighborhood deprivation (i.e., the ADI index).

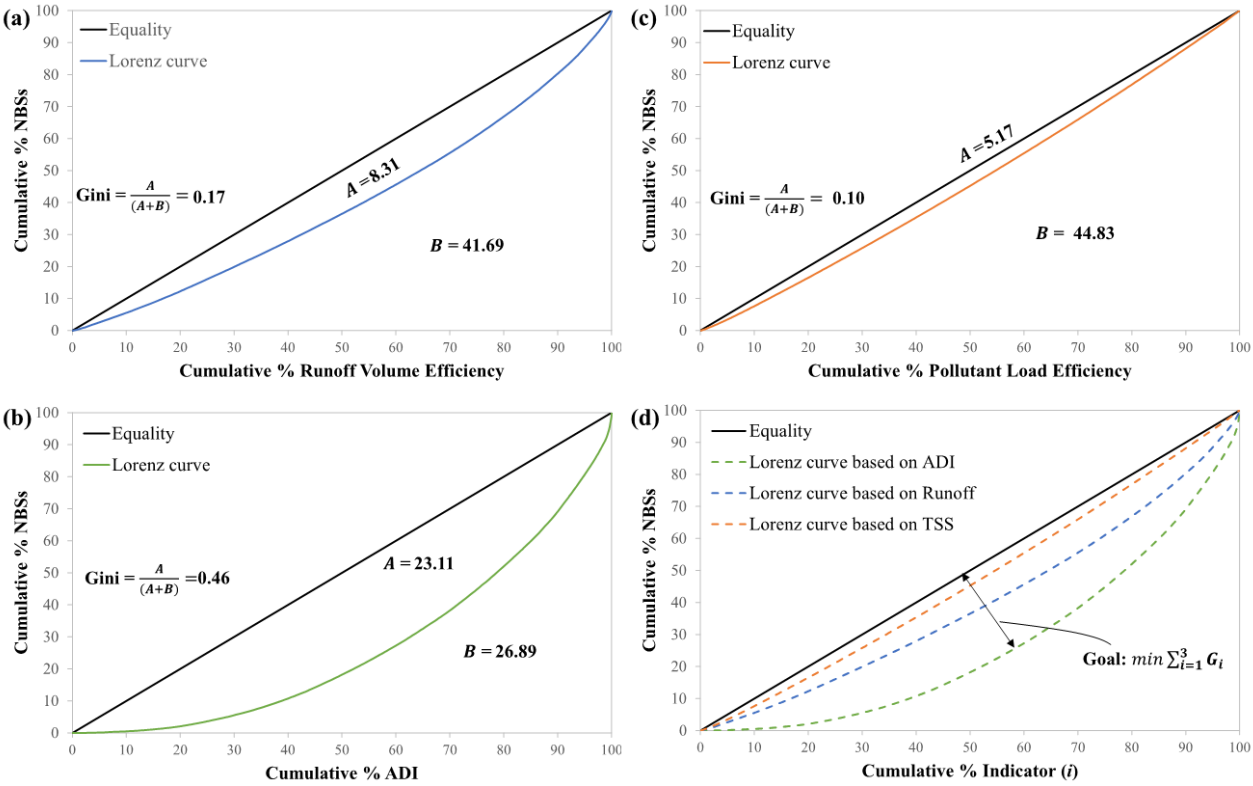

Figure 5. Gini coefficients for Generation 97, Population 117 based on **(a)** runoff volume efficiency, **(b)** pollutant load efficiency, **(c)** Area Deprivation Index, and **(d)** cumulative indicators.

A sample set of outputs from the GreenPlan-IT tool was selected from the 5-YR storm event, each resulting in a total NBS implementation cost of ~$1,000M, to assess how the optimal allocation scheme may shift when the multi-objective Gini coefficient is applied. As shown in **Figure6** and summarized in **Table 1**, a series of 10 possible NBS planning scenarios were evaluated on the basis of the composite Gini coefficient for hydrologic, environmental, and social indicators. By comparing the width of the Lorenz curves and minimizing the total Gini coefficient between these scenarios, **Figure6** reveals that the greatest distribution of equality occurs in planning scenario Generation 22, Population 246. The ideal Gini-based scheme provides a more equal distribution of overall benefits in comparison to the optimal scenario based solely on SWMM modeling (G_i=0.67 in Generation 22, Population 246 and G_i=0.73 in Generation 97, Population 117), despite a similar investment in financial resources. The construction of a multi-objective Lorenz curve is demonstrated here as a simple plot of cumulative NBS spatial allocation against cumulative evaluation indicators (**Figure6**), allowing for easily interpretable comparisons across planning scenarios. The area between the Lorenz curve and the diagonal is proposed as a holistic

index of socio-environmental-hydrological benefits in NBS planning. A larger area below the Lorenz curve suggests that the risk of stormwater-based metrics and social-based metrics are more variable within the planning paradigm, while a smaller area under the curve indicates a more uniform distribution of spatial planning for achieving multiple objectives. The Gini index is a straightforward calculation that could be used in NBS planning to merge holistic benefits using simple algebra. Since the coefficient of derivation under the Lorenz curve is calculated as a standard deviation according to the coefficient of variation, variation is relative, and thus invariant to changes in spatial scale. In other words, the Gini index provides a transparent measurement tool of the summary of impact fractions for optimal planning (Lee, 1997).

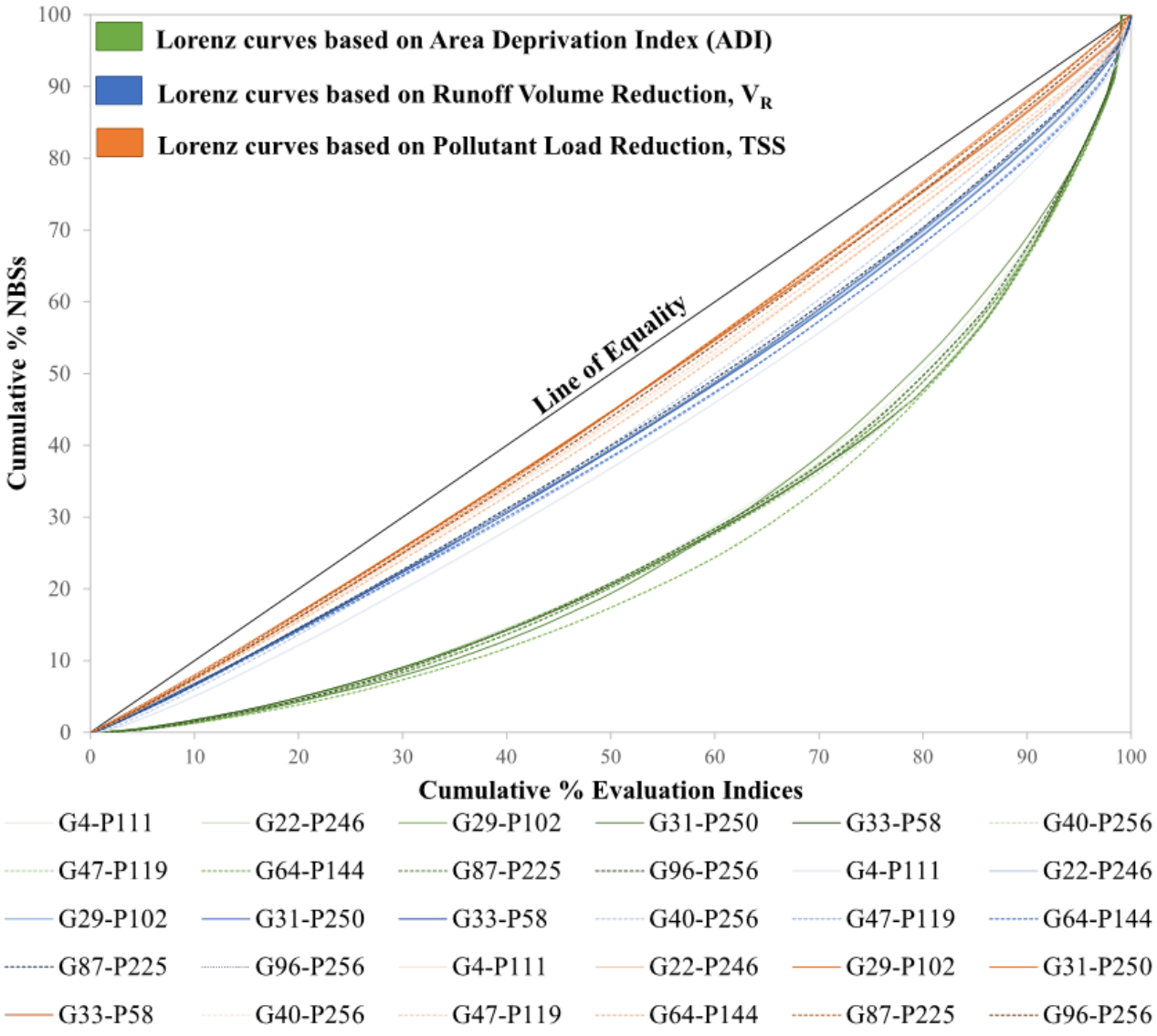

Figure 6. Series of Lorenz curves for select 5-YR, ~$1,000M optimization models.

Table 1. Multi-objective Gini coefficients for select 5-YR storm optimization series.

Gen **Pop**	**G4** **P111**	**G22** **P246**	**G29** **P102**	**G31** **P250**	**G33** **P58**	**G40** **P256**	**G47** **P119**	**G64** **P144**	**G87** **P225**	**G96** **P256**
G_{ADI}	0.436	0.443	0.448	0.442	0.449	0.455	0.444	0.482	0.452	0.442
G_{VR}	0.210	0.157	0.161	0.158	0.163	0.146	0.179	0.178	0.150	0.155
G_{TSS}	0.108	0.072	0.078	0.074	0.080	0.081	0.097	0.112	0.073	0.086
$\sum G_i$	0.753	0.671	0.687	0.674	0.692	0.683	0.721	0.773	0.676	0.683

The optimal allocation of NBSs throughout the planning area may now be adjusted according to the results of the composite Gini coefficient. In **Figure7**, the spatial distribution of NBS allocation according to SWMM-based optimization (i.e., Generation 97, Population 117, from the Pareto front curve) is compared to the spatial distribution of NBSs from the Gini-based optimization (i.e., Generation 22, Population 246, from the minimized composite G_i). By plotting the subcatchments in each scenario as a weighted proportion of NBSs to ADI deprivation, **Figure7d** demonstrates a higher influence of NBS area on the allocation of social equity in the Gini-based scheme, thereby promoting improved societal conditions while maintaining robust hydro-environmental efficiency. As summarized in **Table 2**, both allocation scenarios produce similar runoff volume and pollutant load reduction benefits for roughly the same implementation cost. However, the unique spatial allocation of the NBS features within the Gini-based scenario addresses an additional 18.48% of land areas with high neighborhood disadvantage, as measured by the ADI index.

Table 2. Comparison of SWMM-based optimized model versus Gini-based optimized model.

	G97 **P117**	**G22** **P246**
Cost ($M)	$1006	$1000
Runoff Volume Reduction	3.45%	3.38%
Pollutant Load Reduction	11.15%	11.28%
No. Bioretention Cells	168,459	189,385
No. Porous Pavements	8,705	7,772
No. Tree Boxes	239,001	154,824
% ADI Addressed by NBSs	16.84%	35.32%

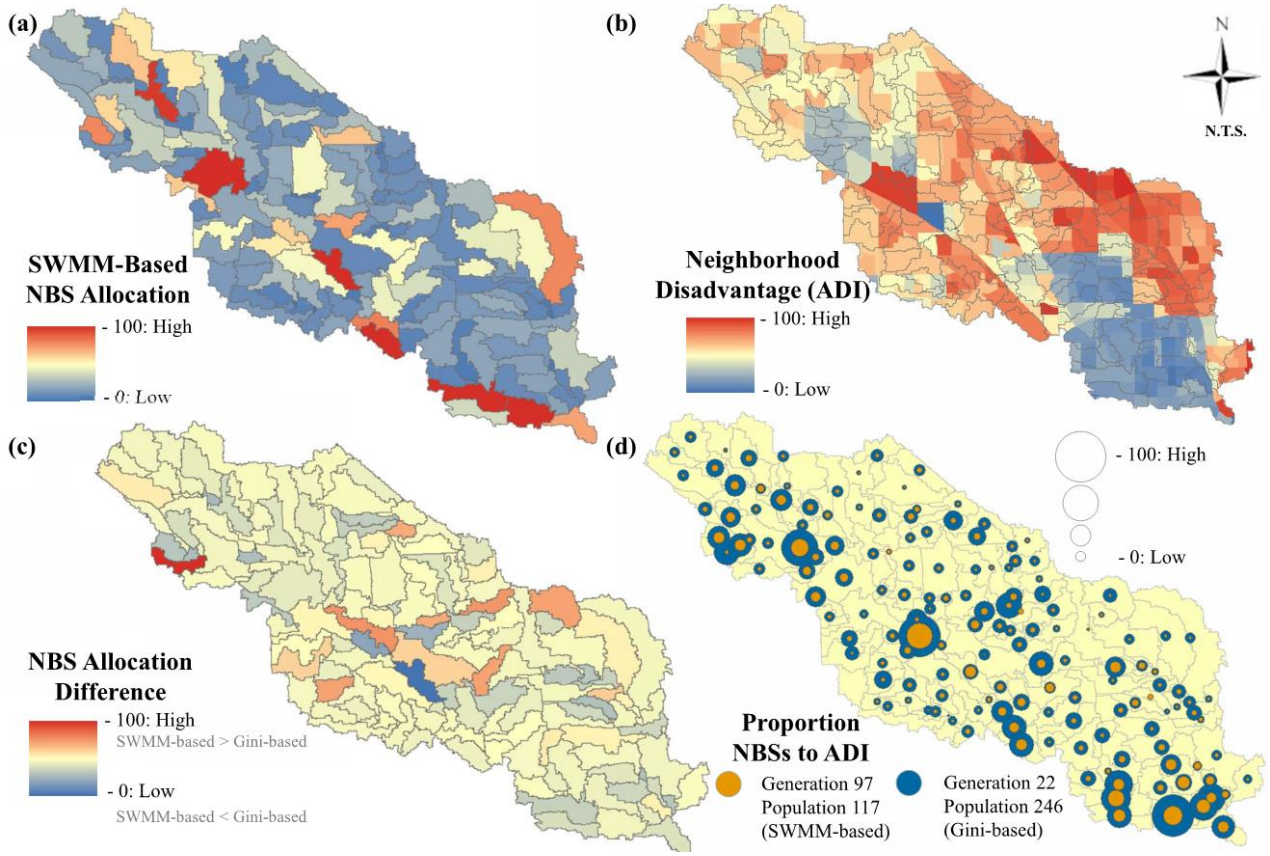

572

573 **Figure 7.** Comparison of spatial distribution in the WOB watershed for **(a)** NBS allocation
574 according to optimal hydro-environmental efficiency (Generation 97, Population 117), **(b)** areas
575 of neighborhood disadvantage, represented by the Area Deprivation Index (ADI), **(c)** difference
576 between NBS allocation for SWMM-based optimization (Generation 97, Population 117) versus
577 Gini-based optimization (Generation 22, Population 246), and **(d)** weighted proportion of NBS
578 allocation within each subcatchment compared to ADI deprivation metrics.

579 The pattern of total allocation of benefits between the SWMM-based and the Gini-based
580 framework is further demonstrated in Error! Reference source not found.**S.5**, where the pie charts
581 represent the weighted efficiency achieved in each subcatchment according to hydrologic,
582 environmental, and social aspects. The green portions of the pie charts in Error! Reference source
583 not found.**S.5** reveals a greater influence of NBS allocation to ADI improvement in Generation 22,
584 Population 246. The primary reason for this disparity is that areas highly prone to flooding or
585 environmental quality issues are not always spatially proportional to areas of high social
586 deprivation. As such, reliance upon a "worst-first" approach to NBS planning through the lens of
587 hydro-dynamics may result in non-optimal allocation for addressing the many societal benefits
588 provided by NBS solutions.

4 Conclusions

As resilience and sustainability goals have become increasingly linked, many governmental agencies are seeking the prioritization of NBS capital improvement projects using an equity-based or benefits-based prioritization metric to help guide equitable investments rather than focusing in a one dimensional benefit (Marchese et al., 2018). To amalgamate such inter-woven goals, decision-makers seek the ability to identify priority planning areas according to the culmination of socio-enviro-hydro processes, which interact within NBS systems to simultaneously enhance both environmental challenges and social health vulnerabilities. Interventions and policies that acclaim to provide social health benefits, but which do not explicitly consider the spatial distribution of social health characteristics within their planning paradigms may be ineffective.

NBS design is a function of rapid urban development, quality of life goals, and a scarcity of resources for addressing hydro-meteorological challenges. As such, proper co-development of NBS plans can and should account for the multifunctional components involved in all of these processes, and we must do so in a coherent fashion for optimal impact in the coming era of water science. In this light, strategic NBS planning requires real-world empirical datasets to aid in clarifying causality amongst disparate social and physical domains in a manner that is understandable and usable by diverse parties to inform interventions for long-term resilience (Frantzeskaki et al., 2019).

By solely relying on hydro-environmental modeling, the relative benefits addressed by NBS solutions are limited and are not able to be optimized according to unique exposures of socio-economic and health-related conditions. Improving resiliency begins with valuing the entangled nature of social well-being and water dynamics. The framework presented here converts hydro-environmental risk and social disparity into a common unit for comparison to adequately capture variation across spatial domains. The Gini index and Lorenz curve are presented as an alternative fundamental approach for optimal NBS planning. This study demonstrates how NBS strategies may be optimized holistically by assessing unique scenarios and minimizing the Gini coefficient across three disparate, but equally important, domains of NBS systems using existing tools and methods in a novel way. As we continue to have increased access to high-resolution spatial datasets, the composite Gini coefficient maximizes our understanding of regional risks and benefits to answer challenging questions associated with multi-functional planning.

We demonstrate here how real-world social and hydro-environmental complexities may be amalgamated using a novel application of the area Gini coefficient for actionable science. This case study investigates how social equity and watershed dynamics propagate throughout the NBS system, which is fundamental to planning for an equitable environment. We harmonize risk-based planning by facilitating an explicit integration of social determinants within the framework of natural-planning using data-driven science. This research transitions beyond the standard focus of watershed physiological characteristics to investigate the complex associations relating social patterns and watershed efficiency. By constructing models with inter-disciplinary elements, we strengthen the foundation for novel research regarding how NBSs function in diverse geographical locations, each with unique properties.

The vision for the future is that we will approach these issues with a systems mindset and transition from our dependency on linear thinking. In the era of the Anthropocene, change is occurring rapidly, and we must better understand complex socio-hydrological systems as necessary for addressing variability in climate and human patterns. Instead of attempting to super-impose human dynamics on the results of physical models, or as a pre-existing boundary condition, we are transitioning toward coupled modeling frameworks that integrate human characteristics as a stimulus that interacts with the environment (Bouziotas & Ertsen, 2017). While coupled social and physical models have proliferated within the general realm of water security (e.g., droughts, water use, hydro-meteorological hazards, migration, agriculture, etc.), the foundation of such a framework has been hitherto lacking within the NBS scientific literature. In considering the rising popularity of urban green infrastructure, we are presented with an opportunity to re-cast how decision-making operates in order to maximize the numerous co-benefits associated with NBSs.

The practical implications of this research will enhance the user-friendliness of NBS spatial planning in a flexible manner while merging well-established hydrological methodologies with a NBS social functionalities (Kuller et al., 2017). When we are better able to select the optimal location of NBSs at a large-scale, the specific typologies and precise placement may be analyzed using the numerous platforms that currently operate through small-scale physical modeling. To date, there has been very little research on NBS optimization at the catchment-scale and even less progress in combining numerical modeling with comprehensive social benefits and human impacts. This study successfully integrates various types of NBS co-benefits into one inter-related framework that combines stormwater abatement, pollutant load modeling, cost-efficiency, and

social equity-based decision-making for robust spatial optimization of NBS systems at the catchment-scale.

By constructing models with inter-disciplinary elements, the foundation for novel research regarding how NBSs function in diverse geographical locations is strengthened. Coupled human-earth models allow for an improved understanding of how social characteristics correlate with environmental processes as a socio-technological system. In a world with increasing socio-environmental stressors and finite resources, this research will improve public policy interventions by providing the knowledge necessary for identifying, quantifying, and linking complex interactions of NBS functions for sound decision-making. Nature-based solutions are expected to become a central tool for climate change adaptation, and we necessitate enhanced approaches to synchronize resiliency goals associated with societal well-being, environmental justice, and natural hazard mitigation through the informed use of NBSs.

Acknowledgments

The author gratefully acknowledges the efforts provided by Dr. Tan Zi of the San Francisco Estuary Institute (SFEI) for troubleshooting the GreenPlan-IT optimization tool to allow application to a large regional watershed in Houston, TX, USA. The author does not perceive any financial conflicts of interest.

Author Contributions

Cyndi V. Castro: Conceptualization; Data curation; Formal analysis; Investigation; Methodology; Project administration; Resources; Software; Visualization; Writing-original draft; Writing-review & editing.

Data Availability Statement

The modeling data used for this study is openly available in the Zenodo data repository, DOI: 10.5281/zenodo.5676315.

References

Addala, A., Auzanneau, M., Miller, K., Maier, W., Foster, N., Kapellen, T., et al. (2021). A decade of disparities in diabetes technology use and HBA1c in pediatric type 1 diabetes: A transatlantic comparison. *Diabetes Care*, *44*(1). https://doi.org/10.2337/dc20-0257

Adib, M., & Wu, H. (2020). Fostering community-engaged green stormwater infrastructure through the use of participatory geographic information systems (PGIS). *Journal of Digital Landscape Architecture*, *2020*(5). https://doi.org/10.14627/537690056

Alves, A., Gersonius, B., Kapelan, Z., Vojinovic, Z., & Sanchez, A. (2019). Assessing the Co-Benefits of green-blue-grey infrastructure for sustainable urban flood risk management. *Journal of Environmental Management*, *239*. https://doi.org/10.1016/j.jenvman.2019.03.036

Astell-Burt, T., & Feng, X. (2021). Urban green space, tree canopy and prevention of cardiometabolic diseases: A multilevel longitudinal study of 46 786 Australians. *International Journal of Epidemiology*, *49*(3). https://doi.org/10.1093/IJE/DYZ239

Barco, J., Wong, K. M., & Stenstrom, M. K. (2009). Closure to "Automatic Calibration of the US EPA SWMM Model for a Large Urban Catchment" by Janet Barco, Kenneth M. Wong, and Michael K. Stenstrom. *Journal of Hydraulic Engineering*, *135*(12). https://doi.org/10.1061/(asce)hy.1943-7900.0000121

Barrett, D. (2019). NOAA Atlas 14 PCPM IDF Curves Update. American Council of Engineering (ACEC) Houston. Retrieved from https://acechouston.org/wp-content/uploads/2017/10/HDR-IDF-Curves-Memo.pdf

Bernagros, J. T., Pankani, D., Struck, S. D., & Deerhake, M. E. (2021). Estimating Regionalized Planning Costs of Green Infrastructure and Low-Impact Development Stormwater Management Practices: Updates to the US Environmental Protection Agency's National Stormwater Calculator. *Journal of Sustainable Water in the Built Environment*, *7*(2). https://doi.org/10.1061/jswbay.0000934

Blair, P., & Buytaert, W. (2016). Socio-hydrological modelling: A review asking "why, what and how?" *Hydrology and Earth System Sciences*, *20*(1). https://doi.org/10.5194/hess-20-443-2016

van den Bosch, M., & Ode Sang. (2017). Urban natural environments as nature-based solutions for improved public health – A systematic review of reviews. *Environmental Research*, *158*. https://doi.org/10.1016/j.envres.2017.05.040

Bouziotas, D., & Ertsen, M. (2017). Socio-hydrology from the bottom up: A template for agent-based modeling in irrigation systems. *Hydrology and Earth System Sciences Discussions*. https://doi.org/10.5194/hess-2017-107

Boyce, J. K., Zwickl, K., & Ash, M. (2016). Measuring environmental inequality. *Ecological Economics*, *124*. https://doi.org/10.1016/j.ecolecon.2016.01.014

Brown, S. C., Lombard, J., Wang, K., Byrne, M. M., Toro, M., Plater-Zyberk, E., et al. (2016). Neighborhood greenness and chronic health conditions in medicare beneficiaries. *American Journal of Preventive Medicine*, *51*(1). https://doi.org/10.1016/j.amepre.2016.02.008

Castro, C. V., & Maidment, D. R. (2020). GIS preprocessing for rapid initialization of HEC-HMS hydrological basin models using web-based data services. *Environmental Modelling and Software*, *130*. https://doi.org/10.1016/j.envsoft.2020.104732

Chamberlain, A. M., Finney Rutten, L. J., Wilson, P. M., Fan, C., Boyd, C. M., Jacobson, D. J., et al. (2020). Neighborhood socioeconomic disadvantage is associated with multimorbidity in a geographically-defined community. *BMC Public Health*, *20*(1). https://doi.org/10.1186/s12889-019-8123-0

719 Chen, C. W., & Shubinski, R. P. (1971). Computer Simulation of Urban Storm Water Runoff. *Journal of*
720 *the Hydraulics Division*, *97*(2). https://doi.org/10.1061/jyceaj.0002871

721 CHI. (2014). PCSWMM Support: Transect creator. Computational Hydraulics International. Retrieved
722 from https://support.chiwater.com/79610/transect-creator

723 CHI. (2015). PCSWMM User's Manual Support: Sensitivity-based Radio Tuning Calibration (SRTC).
724 Computational Hydraulics International. Retrieved from https://support.chiwater.com/78922/srtc

725 CHI. (2020). PCSWMM Support Manual: Error Functions. Computational Hydraulics International.
726 Retrieved from https://support.chiwater.com/79652/error-functions

727 Cho, J. H., & Lee, J. H. (2014). Multi-objective waste load allocation model for optimizing waste load
728 abatement and inequality among waste dischargers. *Water, Air, and Soil Pollution*, *225*(3).
729 https://doi.org/10.1007/s11270-014-1892-2

730 Choi, K. S., & Ball, J. E. (2002). Parameter estimation for urban runoff modelling. *Urban Water*, *4*(1).
731 https://doi.org/10.1016/S1462-0758(01)00072-3

732 Clary, J., Leisenring, M., & Strecker, E. (2020). International Stormwater BMP Database: 2020 Summary
733 Statistics. International Stormwater BMP Database. Retrieved from
734 https://www.waterrf.org/system/files/resource/2020-11/DRPT-4968_0.pdf

735 COH. (2019a). City of Houston Design Manual: Chapter 9, Stormwater Design Requirements, Section
736 9.15. City of Houston Public Works. Retrieved from https://acechouston.org/wp-
737 content/uploads/2019/03/ch-9-including-ch13-2019.pdf

738 COH. (2019b). Infrastructure Design Manual 2019, Section 9.2.01.B.1, Design Rainfall Events. City of
739 Houston Public Works. Retrieved from
740 https://www.houstonpermittingcenter.org/media/4121/download

741 COH. (2021). City of Houston Data Hub. City of Houston. Retrieved from https://cohgis-
742 mycity.opendata.arcgis.com/

743 Deb, K., Pratap, A., Agarwal, S., & Meyarivan, T. (2002). A fast and elitist multiobjective genetic
744 algorithm: NSGA-II. *IEEE Transactions on Evolutionary Computation*, *6*(2).
745 https://doi.org/10.1109/4235.996017

746 Despart, Z. (2019). Harris County approves "worst-first" priority model for flood bond projects. Houston
747 Chronicle. Retrieved from https://www.houstonchronicle.com/news/houston-
748 texas/houston/article/Harris-County-approves-worst-first-priority-14383015.php

749 Druckman, A., & Jackson, T. (2008). Measuring resource inequalities: The concepts and methodology for
750 an area-based Gini coefficient. *Ecological Economics*, *65*(2).
751 https://doi.org/10.1016/j.ecolecon.2007.12.013

752 Du, E., Cai, X., Wu, F., Foster, T., & Zheng, C. (2021). Exploring the impacts of the inequality of water
753 permit allocation and farmers' behaviors on the performance of an agricultural water market.
754 *Journal of Hydrology*, *599*. https://doi.org/10.1016/j.jhydrol.2021.126303

755 Eckart, K., McPhee, Z., & Bolisetti, T. (2017). Performance and implementation of low impact
756 development – A review. *Science of the Total Environment*.
757 https://doi.org/10.1016/j.scitotenv.2017.06.254

758 Fenner, R. (2017). Spatial evaluation of multiple benefits to encourage multi-functional design of
759 sustainable drainage in Blue-Green cities. *Water (Switzerland)*, *9*(12).
760 https://doi.org/10.3390/w9120953

761 Flanagan, B. E., Gregory, E. W., Hallisey, E. J., Heitgerd, J. L., & Lewis, B. (2020). A Social
762 Vulnerability Index for Disaster Management. *Journal of Homeland Security and Emergency*

763 *Management*, *8*(1). https://doi.org/10.2202/1547-7355.1792

764 Frantzeskaki, N., McPhearson, T., Collier, M. J., Kendal, D., Bulkeley, H., Dumitru, A., et al. (2019).
765 Nature-based solutions for urban climate change adaptation: Linking science, policy, and practice
766 communities for evidence-based decision-making. *BioScience*, *69*(6).
767 https://doi.org/10.1093/biosci/biz042

768 Fuertes, E., Markevych, I., von Berg, A., Bauer, C. P., Berdel, D., Koletzko, S., et al. (2014). Greenness
769 and allergies: Evidence of differential associations in two areas in Germany. *Journal of*
770 *Epidemiology and Community Health*, *68*(8). https://doi.org/10.1136/jech-2014-203903

771 Gascon, M., Triguero-Mas, M., Martínez, D., Dadvand, P., Rojas-Rueda, D., Plasència, A., &
772 Nieuwenhuijsen, M. J. (2016). Residential green spaces and mortality: A systematic review.
773 *Environment International*. https://doi.org/10.1016/j.envint.2015.10.013

774 Gini, C. W. (1912). Variability and Mutability, contribution to the study of statistical distributions and
775 relations. *Studi Economico-Giuridici Della Studi Economico-Giuricici Della R. Università de*
776 *Cagliari*.

777 Giorgi, G. M., & Gigliarano, C. (2017). THE GINI CONCENTRATION INDEX: A REVIEW OF THE
778 INFERENCE LITERATURE. *Journal of Economic Surveys*, *31*(4).
779 https://doi.org/10.1111/joes.12185

780 Golden, H. E., & Hoghooghi, N. (2018). Green infrastructure and its catchment-scale effects: an emerging
781 science. *Wiley Interdisciplinary Reviews: Water*, *5*(1). https://doi.org/10.1002/wat2.1254

782 Groves-Kirkby, C. J., Denman, A. R., & Phillips, P. S. (2009). Lorenz Curve and Gini Coefficient: Novel
783 tools for analysing seasonal variation of environmental radon gas. *Journal of Environmental*
784 *Management*, *90*(8). https://doi.org/10.1016/j.jenvman.2009.01.003

785 Hamouz, V., Møller-Pedersen, P., & Muthanna, T. M. (2020). Modelling runoff reduction through
786 implementation of green and grey roofs in urban catchments using PCSWMM. *Urban Water*
787 *Journal*, *17*(9). https://doi.org/10.1080/1573062X.2020.1828500

788 HCFCD. (2019). Model and map management system (M3). *Harris County Flood Control District*.
789 Retrieved from https://www.m3models.org/

790 HCFCD. (2021). Harris County Flood Warning System. Harris County Flood Control District. Retrieved
791 from https://www.harriscountyfws.org/

792 Heerink, N., Mulatu, A., & Bulte, E. (2001). Income inequality and the environment: Aggregation bias in
793 environmental Kuznets curves. *Ecological Economics*, *38*(3). https://doi.org/10.1016/S0921-
794 8009(01)00171-9

795 Hirshberg, E. L., Wilson, E. L., Stanfield, V., Kuttler, K. G., Majercik, S., Beesley, S. J., et al. (2019).
796 Impact of Critical Illness on Resource Utilization: A Comparison of Use in the Year Before and
797 After ICU Admission. *Critical Care Medicine*, *47*(11).
798 https://doi.org/10.1097/CCM.0000000000003970

799 Hu, Z., Chen, Y., Yao, L., Wei, C., & Li, C. (2016). Optimal allocation of regional water resources: From
800 a perspective of equity-efficiency tradeoff. *Resources, Conservation and Recycling*, *109*.
801 https://doi.org/10.1016/j.resconrec.2016.02.001

802 Ingraham, N. E., Purcell, L. N., Karam, B. S., Dudley, R. A., Usher, M. G., Warlick, C. A., et al. (2021).
803 Racial and Ethnic Disparities in Hospital Admissions from COVID-19: Determining the Impact of
804 Neighborhood Deprivation and Primary Language. *Journal of General Internal Medicine*.
805 https://doi.org/10.1007/s11606-021-06790-w

806 Jacobson, A., Milman, A. D., & Kammen, D. M. (2005). Letting the (energy) Gini out of the bottle:
807 Lorenz curves of cumulative electricity consumption and Gini coefficients as metrics of energy

distribution and equity. *Energy Policy*, *33*(14). https://doi.org/10.1016/j.enpol.2004.02.017

James, W. (2003). Rules for responsible modeling. Computational Hydraulics International. Retrieved from https://www.chiwater.com/Files/R184_CHI_Rules.pdf

Jato-Espino, D., Charlesworth, S. M., Bayon, J. R., & Warwick, F. (2016). Rainfall-runoff simulations to assess the potential of suds for mitigating flooding in highly urbanized catchments. *International Journal of Environmental Research and Public Health*, *13*(1). https://doi.org/10.3390/ijerph13010149

Josa, I., & Aguado, A. (2020). Measuring Unidimensional Inequality: Practical Framework for the Choice of an Appropriate Measure. *Social Indicators Research*, *149*(2). https://doi.org/10.1007/s11205-020-02268-0

Kabisch, N., Frantzeskaki, N., Pauleit, S., Naumann, S., Davis, M., Artmann, M., et al. (2016). Nature-based solutions to climate change mitigation and adaptation in urban areas: Perspectives on indicators, knowledge gaps, barriers, and opportunities for action. *Ecology and Society*, *21*(2). https://doi.org/10.5751/ES-08373-210239

Kandakoglu, A., Frini, A., & Ben Amor, S. (2019). Multicriteria decision making for sustainable development: A systematic review. *Journal of Multi-Criteria Decision Analysis*, *26*(5–6). https://doi.org/10.1002/mcda.1682

Kind, A. J. H., & Buckingham, W. R. (2018). Making Neighborhood-Disadvantage Metrics Accessible — The Neighborhood Atlas. *New England Journal of Medicine*, *378*(26). https://doi.org/10.1056/nejmp1802313

Knighton, A. J., Savitz, L., Belnap, T., Stephenson, B., & VanDerslice, J. (2016). Introduction of an Area Deprivation Index Measuring Patient Socio-economic Status in an Integrated Health System: Implications for Population Health. *EGEMs (Generating Evidence & Methods to Improve Patient Outcomes)*, *4*(3). https://doi.org/10.13063/2327-9214.1238

Koutsoyiannis, D., Kozonis, D., & Manetas, A. (1998). A mathematical framework for studying rainfall intensity-duration-frequency relationships. *Journal of Hydrology*, *206*(1–2). https://doi.org/10.1016/S0022-1694(98)00097-3

Kuil, L., Carr, G., Viglione, A., Prskawetz, A., & Blöschl, G. (2016). Conceptualizing socio-hydrological drought processes: The case of the Maya collapse. *Water Resources Research*, *52*(8). https://doi.org/10.1002/2015WR018298

Kuller, M., Bach, P. M., Ramirez-Lovering, D., & Deletic, A. (2017). Framing water sensitive urban design as part of the urban form: A critical review of tools for best planning practice. *Environmental Modelling and Software*. https://doi.org/10.1016/j.envsoft.2017.07.003

Kurani, S. S., McCoy, R. G., Lampman, M. A., Doubeni, C. A., Finney Rutten, L. J., Inselman, J. W., et al. (2020). Association of Neighborhood Measures of Social Determinants of Health With Breast, Cervical, and Colorectal Cancer Screening Rates in the US Midwest. *JAMA Network Open*, *3*(3). https://doi.org/10.1001/jamanetworkopen.2020.0618

Lee, W. C. (1997). Characterizing exposure-disease association in human populations using the Lorenz curve and Gini index. *Statistics in Medicine*, *16*(7). https://doi.org/10.1002/(SICI)1097-0258(19970415)16:7<729::AID-SIM491>3.0.CO;2-A

Li, H., Ding, L., Ren, M., Li, C., & Wang, H. (2017). Sponge city construction in China: A survey of the challenges and opportunities. *Water (Switzerland)*, *9*(9). https://doi.org/10.3390/w9090594

Lim, T. C., & Welty, C. (2017). Effects of spatial configuration of imperviousness and green infrastructure networks on hydrologic response in a residential sewershed. *Water Resources Research*, *53*(9). https://doi.org/10.1002/2017WR020631

Lin, J. (2004). Review of published export coefficient and event mean concentration (EMC) data: ERDC TN-WRAP-04-3. Wetlands Regulatory Assistance Program. Retrieved from https://apps.dtic.mil/dtic/tr/fulltext/u2/a430436.pdf

Link, B. G., & Phelan, J. (1995). Social conditions as fundamental causes of disease. *Journal of Health and Social Behavior*. https://doi.org/10.2307/2626958

Liu, L., & Jensen, M. B. (2018). Green infrastructure for sustainable urban water management: Practices of five forerunner cities. *Cities*, *74*. https://doi.org/10.1016/j.cities.2017.11.013

Liu, Yang, Wang, C., Yu, Y., Chen, Y., Du, L., Qu, X., et al. (2019). Effect of urban stormwater road runoffof different land use types on an urban river in Shenzhen, China. *Water (Switzerland)*, *11*(12). https://doi.org/10.3390/w11122545

Liu, Yaoze, Ahiablame, L. M., Bralts, V. F., & Engel, B. A. (2015). Enhancing a rainfall-runoff model to assess the impacts of BMPs and LID practices on storm runoff. *Journal of Environmental Management*, *147*. https://doi.org/10.1016/j.jenvman.2014.09.005

Loperfido, J. V., Noe, G. B., Jarnagin, S. T., & Hogan, D. M. (2014). Effects of distributed and centralized stormwater best management practices and land cover on urban stream hydrology at the catchment scale. *Journal of Hydrology*, *519*(PC). https://doi.org/10.1016/j.jhydrol.2014.07.007

Ludwig, J., Sanbonmatsu, L., Gennetian, L., Adam, E., Duncan, G. J., Katz, L. F., et al. (2011). Neighborhoods, Obesity, and Diabetes — A Randomized Social Experiment. *New England Journal of Medicine*, *365*(16). https://doi.org/10.1056/nejmsa1103216

Maas, J., van Dillen, S. M. E., Verheij, R. A., & Groenewegen, P. P. (2009). Social contacts as a possible mechanism behind the relation between green space and health. *Health and Place*, *15*(2). https://doi.org/10.1016/j.healthplace.2008.09.006

Madureira, H., & Andresen, T. (2014). Planning for multifunctional urban green infrastructures: Promises and challenges. *Urban Design International*, *19*(1). https://doi.org/10.1057/udi.2013.11

Marchese, D., Reynolds, E., Bates, M. E., Morgan, H., Clark, S. S., & Linkov, I. (2018). Resilience and sustainability: Similarities and differences in environmental management applications. *Science of the Total Environment*. https://doi.org/10.1016/j.scitotenv.2017.09.086

Martikainen, P., Mäki, N., & Blomgren, J. (2004). The effects of area and individual social characteristics on suicide risk: A multilevel study of relative contribution and effect modification. *European Journal of Population*, *20*(4). https://doi.org/10.1007/s10680-004-3807-1

Van de Meene, S. J., Brown, R. R., & Farrelly, M. A. (2011). Towards understanding governance for sustainable urban water management. *Global Environmental Change*, *21*(3). https://doi.org/10.1016/j.gloenvcha.2011.04.003

Mitchell, R., & Popham, F. (2008). Effect of exposure to natural environment on health inequalities: an observational population study. *The Lancet*, *372*(9650). https://doi.org/10.1016/S0140-6736(08)61689-X

Nkoy, F. L., Stone, B. L., Knighton, A. J., Fassl, B. A., Johnson, J. M., Maloney, C. G., & Savitz, L. A. (2018). Neighborhood Deprivation and Childhood Asthma Outcomes, Accounting for Insurance Coverage. *Hospital Pediatrics*, *8*(2). https://doi.org/10.1542/hpeds.2017-0032

Pande, S., & Sivapalan, M. (2017). Progress in socio-hydrology: a meta-analysis of challenges and opportunities. *Wiley Interdisciplinary Reviews: Water*, *4*(4). https://doi.org/10.1002/wat2.1193

Perez-Pedini, C., Limbrunner, J. F., & Vogel, R. M. (2005). Optimal Location of Infiltration-Based Best Management Practices for Storm Water Management. *Journal of Water Resources Planning and Management*, *131*(6). https://doi.org/10.1061/(asce)0733-9496(2005)131:6(441)

Perica, S., Pavlovic, S., Laurent, M. St., Trypaluk, C., Unruh, D., & Wilhite, O. (2018). NOAA Atlas 14 Precipitation-Frequency Atlas of the United States Volume 11 Version 2.0: Texas. U.S. Department of Commerce, National Oceanic and Atmospheric Administration, National Weather Service. Retrieved from https://www.weather.gov/media/owp/oh/hdsc/docs/Atlas14_Volume11.pdf

Pitt, R., Maestre, A., & Clary, J. (2015). National Stormwater Quality Database (NSQD), Version 4.02 (2001-2015). International Stormwater BMP Database. Retrieved from https://static1.squarespace.com/static/5f8dbde10268ab224c895ad7/t/5fbd4f842192d61a1f85f71a/1606242187964/NSQD_ver_4_brief_Feb_18_2018.pdf

Ray, H., & Jakubec, S. L. (2014). Nature-based experiences and health of cancer survivors. *Complementary Therapies in Clinical Practice*, *20*(4). https://doi.org/10.1016/j.ctcp.2014.07.005

Rossi, L., Fankhauser, R., & Chèvre, N. (2006). Water quality criteria for total suspended solids (TSS) in urban wet-weather discharges. *Water Science and Technology*, *54*(6–7). https://doi.org/10.2166/wst.2006.623

Rossman, L. (2014). National Stormwater Calculator User's Guide: Version 1.1. Environmental Protection Agency. Retrieved from https://nepis.epa.gov/Adobe/PDF/P100HD4J.pdf

Rossman, L. A., & Huber, W. C. (2016). *Storm Water Management Model User's Manual*. *United States Environment Protection Agency*.

Ruangpan, L., Vojinovic, Z., Di Sabatino, S., Leo, L. S., Capobianco, V., Oen, A. M. P., et al. (2020). Nature-based solutions for hydro-meteorological risk reduction: a state-of-the-art review of the research area. *Natural Hazards and Earth System Sciences*, *20*(1). https://doi.org/10.5194/nhess-20-243-2020

Saboohi, Y. (2001). An evaluation of the impact of reducing energy subsidies on living expenses of households. *Energy Policy*, *29*(3). https://doi.org/10.1016/S0301-4215(00)00116-6

Sadras, V., & Bongiovanni, R. (2004). Use of Lorenz curves and Gini coefficients to assess yield inequality within paddocks. *Field Crops Research*, *90*(2–3). https://doi.org/10.1016/j.fcr.2004.04.003

Sarabi, S., Han, Q., Romme, A. G. L., de Vries, B., Valkenburg, R., & den Ouden, E. (2020). Uptake and implementation of Nature-Based Solutions: An analysis of barriers using Interpretive Structural Modeling. *Journal of Environmental Management*, *270*. https://doi.org/10.1016/j.jenvman.2020.110749

Sarabi, S. E., Han, Q., Romme, A. G. L., de Vries, B., & Wendling, L. (2019). Key enablers of and barriers to the uptake and implementation of nature-based solutions in urban settings: A review. *Resources*. https://doi.org/10.3390/resources8030121

Sarma, P. B. S., Delleur, J. W., & Rao, A. R. (1973). Comparison of rainfall-runoff models for urban areas. *Journal of Hydrology*, *18*(3–4). https://doi.org/10.1016/0022-1694(73)90056-5

Schlossberg, M. (2003). GIS, the US census and neighbourhood scale analysis. *Planning Practice and Research*, *18*(2–3). https://doi.org/10.1080/0269745032000168269

SFEI. (2018). GreenPlanIT Optimization Tool User Manual. San Francisco Estuary Institute. Retrieved from http://greenplanit.sfei.org/sites/default/files/Optimization Tool User Manual 2020.pdf

SFEI. (2020). GreenPlan-IT Case Study: San Jose's Urban Villages, Chapter 3. San Francisco Estuary Institute. Retrieved from https://greenplanit.sfei.org/books/chapter-3-case-study-san-jose's-urban-villages

Singh, G. K. (2003). Area Deprivation and Widening Inequalities in US Mortality, 1969-1998. *American Journal of Public Health*, *93*(7). https://doi.org/10.2105/AJPH.93.7.1137

Sun, T., Zhang, H., Wang, Y., Meng, X., & Wang, C. (2010). The application of environmental Gini coefficient (EGC) in allocating wastewater discharge permit: The case study of watershed total mass control in Tianjin, China. *Resources, Conservation and Recycling*, *54*(9). https://doi.org/10.1016/j.resconrec.2009.10.017

TNRIS. (2019). Harris County LiDAR 2018. Retrieved from https://data.tnris.org/collection/b5bd2b96-8ba5-4dc6-ba88-d88133eb6643

University of Wisconsin School of Medicine and Public. (2019). Area Deprivation Index. Retrieved from https://www.neighborhoodatlas.medicine.wisc.edu/ (August 16, 2021)

USDA. (1986). Urban Hydrology for Small Watersheds: TR-55. United States Department of Agriculture, Natural Resources Conservation Service, Conservation Enginereing Division. Retrieved from https://www.nrcs.usda.gov/Internet/FSE_DOCUMENTS/stelprdb1044171.pdf

USGS. (2021a). USGS 08074020 Whiteoak Bayou at Alabonson Rd, Houston, TX. United States Geological Survey. Retrieved from https://waterdata.usgs.gov/tx/nwis/uv/?site_no=08074020&PARAmeter_cd=00065,00060

USGS. (2021b). USGS 08074500 Whiteoak Bayou at Houston, TX. United States Geological Survey. Retrieved from https://waterdata.usgs.gov/tx/nwis/uv/?site_no=08074500&PARAmeter_cd=00065,00060

Wamsler, C., Wickenberg, B., Hanson, H., Alkan Olsson, J., Stålhammar, S., Björn, H., et al. (2020). Environmental and climate policy integration: Targeted strategies for overcoming barriers to nature-based solutions and climate change adaptation. *Journal of Cleaner Production*, *247*. https://doi.org/10.1016/j.jclepro.2019.119154

White, M., Harmel, D., Yen, H., Arnold, J., Gambone, M., & Haney, R. (2015). Development of Sediment and Nutrient Export Coefficients for U.S. Ecoregions. *Journal of the American Water Resources Association*, *51*(3). https://doi.org/10.1111/jawr.12270

White, T. J. (2007). Sharing resources: The global distribution of the Ecological Footprint. *Ecological Economics*, *64*(2). https://doi.org/10.1016/j.ecolecon.2007.07.024

Wihlborg, M., Sörensen, J., & Alkan Olsson, J. (2019). Assessment of barriers and drivers for implementation of blue-green solutions in Swedish municipalities. *Journal of Environmental Management*, *233*. https://doi.org/10.1016/j.jenvman.2018.12.018

Wu, J., Kauhanen, P. G., Hunt, J. A., Senn, D. B., Hale, T., & McKee, L. J. (2019). Optimal Selection and Placement of Green Infrastructure in Urban Watersheds for PCB Control. *Journal of Sustainable Water in the Built Environment*, *5*(2). https://doi.org/10.1061/jswbay.0000876

Yan, D., Jia, Z., Xue, J., Sun, H., Gui, D., Liu, Y., & Zeng, X. (2018). Inter-regional coordination to improve equality in the agricultural virtualwater trade. *Sustainability (Switzerland)*, *10*(12). https://doi.org/10.3390/su10124561

Yang, L., Jin, S., Danielson, P., Homer, C., Gass, L., Bender, S. M., et al. (2018). A new generation of the United States National Land Cover Database: Requirements, research priorities, design, and implementation strategies. *ISPRS Journal of Photogrammetry and Remote Sensing*, *146*. https://doi.org/10.1016/j.isprsjprs.2018.09.006

Zhang, D., Shen, J., Liu, P., Zhang, Q., & Sun, F. (2020). Use of fuzzy analytic hierarchy process and environmental gini coefficient for allocation of regional flood drainage rights. *International Journal of Environmental Research and Public Health*, *17*(6). https://doi.org/10.3390/ijerph17062063

Zhang, K., & Chui, T. F. M. (2018). A comprehensive review of spatial allocation of LID-BMP-GI practices: Strategies and optimization tools. *Science of the Total Environment*. https://doi.org/10.1016/j.scitotenv.2017.11.281

SUPPLEMENTARY MATERIAL

Optimizing nature-based solutions by combining social equity, hydro-environmental efficiency, and economic costs through a novel Gini coefficient

Cyndi V. Castro

Table S.1. Atlas 14 rainfall coefficients for Houston, Texas, USA.

Rainfall Frequency	b (inches)	d (minutes)	e
2-Year (50% AEP)	47.25	8.94	0.7263
5-Year (20% AEP)	54.09	8.34	0.7051
10-Year (10% AEP)	55.26	7.30	0.6752
25-Year (4% AEP)	56.72	6.12	0.6397
50-Year (2% AEP)	57.94	5.47	0.6166
100-Year (1% AEP)	56.68	4.46	0.5857

Table S.1. Pollutant load parameters for modeling total suspended solids (TSS).

		Removal Efficiency (%)		
Land Use	**TSS** *(mg/L)*	*Porous Pavement*	*Bioretention Cell*	*Tree Box*
Industrial	145.43	60%	50%	50%
Residential	146.00			
Mixed Use	72.93			
Commercial	92.56			
Open Space	211.33			

Table S.2. Water balance zones represented in the WOB case study.

NBS Feature	Surface	Soil	Storage	Underdrain
Porous Pavement	X		X	X
Bioretention Cell	X	X	X	X
Tree Box	X	X	X	

Table S.4. PCSWMM LID Control Editor parameter inputs. BIOR: "Bioretention cell", PMPV: "Permeable pavement", TRBX: "Tree box".

	Parameter	NBS Feature			Units
		BIOR	**PMPV**	**TRBX**	
Surface	Berm height	9	0	12	Inch
	Vegetation volume	0	0	0.2	Fraction
	Surface roughness	0.1	0.1	0.1	-
	Surface slope	1.0	1.0	1.0	Percent
Pavement	Thickness	-	4	-	Inch
	Void ratio	-	0.15	-	Voids/solids
	Impervious surface	-	0	-	Fraction
	Permeability	-	100	-	Inch/hour
Soil	Thickness	18	0	21	Inch
	Porosity	0.5	0.5	0.5	Volume fraction
	Field capacity	0.2	0.2	0.2	Volume fraction
	Wilting point	0.1	0.1	0.1	Volume fraction
	Conductivity	5	0.5	50	Inch/hour
	Conductivity slope	10	10	10	-
	Suction head	3.5	3.5	3.5	Inch
Storage	Thickness	12	24	6	Inch
	Void ratio	0.75	0.75	0.75	Voids/solids
	Seepage rate	0.5	5	0.5	Inch/hour
	Clogging factor	0	0	0	-
Drain	Drain coefficient	5	100	50	Inch/hour
	Drain exponent	0.5	0.5	0.5	-
	Drain offset height	12	8	0	Inch

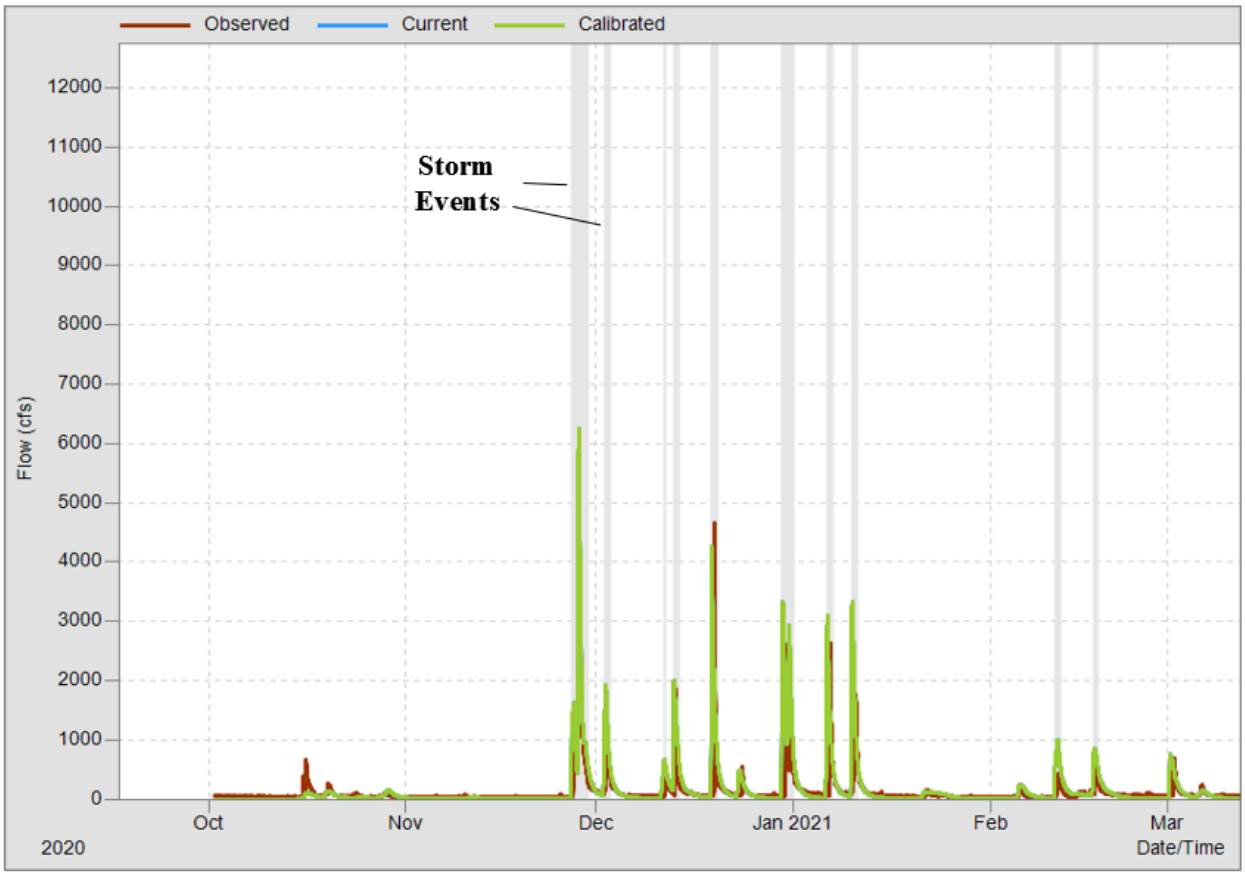

Figure S.1. Sample of storm event selection in PCSWMM.

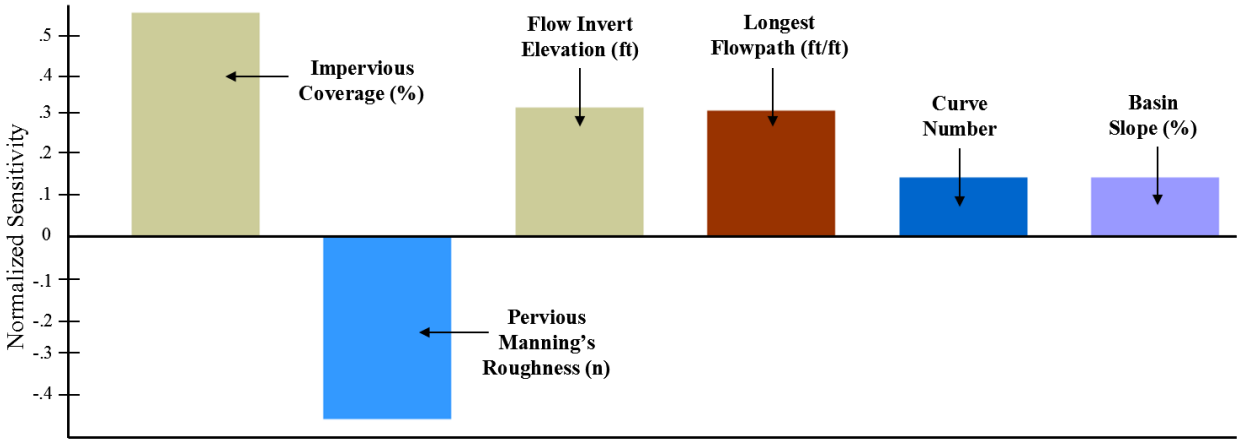

Figure S.2. Normalized sensitivity analysis output for primary variables.

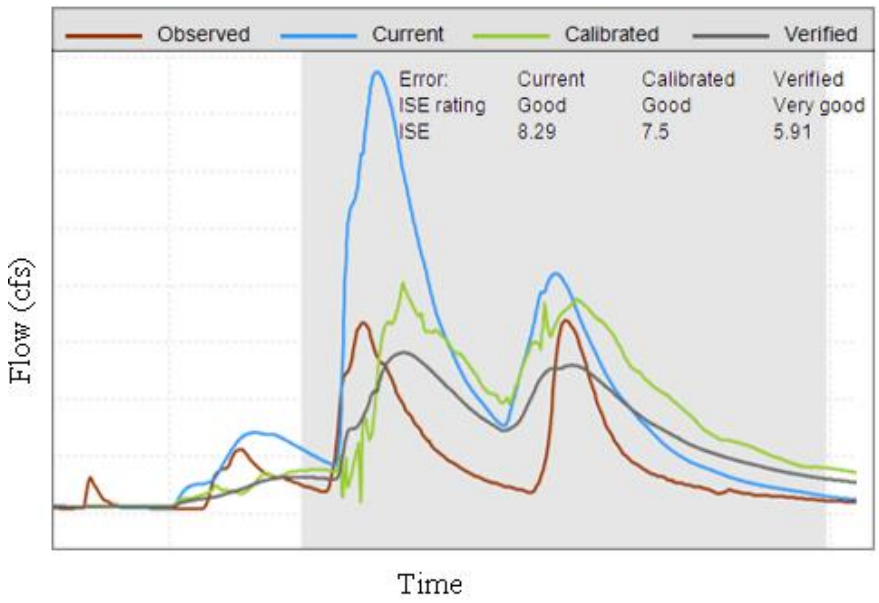

Figure S.3. Validation output hydrographs for select storm event (Mar. 2021 to Aug. 2021).

Table S.5. ISE statistics between simulated and observed flows for calibration.

		Gauge No. 08074500	Gauge No. 08074020
Storm Event No.	Date	Rating (ISE)	
1	Nov. 27, 2020	Good (8.4)	Good (6.3)
2	Dec. 2, 2020	Good (8.9)	Good (10.0)
3	Dec. 11, 2020	Good (9.3)	Fair (11.3)
4	Dec. 13, 2020	Fair (13.7)	Good (6.3)
5	Dec. 19, 2020	Very Good (5.9)	Good (8.3)
6	Dec. 30, 2020	Good (10.0)	Very Good (6.0)
7	Jan. 6, 2021	Good (10.7)	Fair (11.0)
8	Jan. 10, 2021	Good (7.2)	Good (7.5)
9	Feb. 11, 2021	Good (8.3)	Good (7.5)
10	Feb. 17, 2021	Very Good (4.6)	Good (7.1)

Table S.6. ISE statistics between simulated and observed flows for validation.

		Gauge No. 08074500	Gauge No. 08074020
Storm Event No.	Date	Rating (ISE)	
1	Apr. 30, 2021	Very Good (4.7)	Very Good (5.9)
2	May 16, 2021	Very Good (5.9)	Very Good (5.9)
3	May 22, 2021	Very Good (4.8)	Very Good (4.9)
4	Jun. 2, 2021	Good (6.8)	Good (7.6)
5	Jun. 27, 2021	Good (8.8)	Very Good (4.6)
6	Jul. 3, 2021	Very Good (4.5)	Very Good (4.9)
7	Jul. 8, 2021	Very Good (5.2)	Good (9.0)
8	Jul. 15, 2021	Very Good (5.6)	Good (6.4)

Table S.7. GreenPlan-IT Optimization Tool subcatchment input file. BIOR: "Bioretention cell", PMPV: "Permeable pavement", TRBX: "Tree box".

			No. Possible NBS Features		
Subcatchment No.	**Area (AC)**	**Impervious Cover (%)**	**BIOR**	**PMPV**	**TRBX**
1	709.4	43.7	4904	96	7761
2	1420.5	45.4	18158	317	17632
3	683	40.7	8178	37	10573
4	363.1	47.6	1449	43	9745
5	588.5	33.5	6639	229	214
6	358.6	51.5	1815	4	9404
7	712	32.5	17376	93	3208
8	815	46.5	12339	362	4034
9	913	43.7	11430	157	14351
10	432.8	40.9	4932	96	387
11	584.9	52	4521	133	9299
12	62.4	32.6	1385	4	22
13	86.7	47.8	937	0	1984
14	1018.4	34.8	7250	192	11130
15	519.2	50.7	6103	194	8295
16	358.4	33.9	4273	38	3359
17	270.7	54.7	1537	35	8309
18	256.3	59	680	17	10540
19	871.2	59	6796	333	12400
20	300.7	24.7	1780	123	259
21	197.7	59.1	1602	195	231
22	399.5	64.3	3392	313	5719
23	519	31.4	8859	55	0
24	382.5	42.9	3635	183	547
25	226.8	52.6	1843	18	3654
26	447.7	41.8	6841	87	643
27	502.9	59.5	5273	217	7760
28	358.4	39.2	3186	143	168
29	282.3	20.1	4122	10	0
30	614.4	41.7	6045	7	4934
31	42.5	65.9	284	69	154
32	153.3	31.6	3360	0	1519
33	340.4	51.1	6349	341	131
34	83.4	62.3	1074	63	145
35	261.7	44	1175	7	488

Table S.7 (continued):

			No. Possible NBS Features		
Subcatchment No.	**Area (AC)**	**Impervious Cover (%)**	**BIOR**	**PMPV**	**TRBX**
36	458.3	54.5	3629	44	11804
37	966.4	51.6	12159	287	9376
38	279.7	43.4	1746	87	968
39	1004	37.3	5286	31	1553
40	47	28.4	1330	0	105
41	480.7	43.8	6856	215	857
42	169.6	38.6	2098	0	4163
43	391	31.5	1486	13	1441
44	341.4	51.6	5228	174	157
45	413.6	43.5	4583	31	1472
46	69.5	18.6	1041	0	339
47	467.3	49.7	4184	311	302
48	1197.9	51.8	11504	399	16692
49	590.3	52.2	4907	96	14166
50	250.2	53.9	1181	88	6201
51	562	41.4	5508	23	12750
52	549.5	42.9	4888	28	11791
53	312.8	57.8	1122	14	10247
54	333.8	38.6	5519	51	884
55	108.4	39.6	1592	77	0
56	431.6	41.5	4998	8	8551
57	349.6	22.6	3603	30	1829
58	712.5	43.2	5598	60	11214
59	96.6	37.1	1051	0	2461
60	35.2	54.9	443	0	64
61	358.6	37.3	3386	24	6237
62	318.4	63.7	3010	343	866
63	61.4	42.8	352	0	909
64	302.1	42.1	1288	32	2621
65	811.4	47.7	6421	248	6760
66	182.1	49.6	2088	121	2277
67	0.7	13.8	25	0	0
68	326.9	49.4	1317	29	3681
69	1903.1	55.1	13296	1533	18592
70	171.7	61.5	1461	135	1313
71	1017	29.8	21837	97	6886

Table S.7 (continued):

			No. Possible NBS Features		
Subcatchment No.	**Area (AC)**	**Impervious Cover (%)**	**BIOR**	**PMPV**	**TRBX**
73	501.5	39.8	6885	29	3604
74	909.5	55.3	13125	525	3490
75	237.6	73	1157	241	52
76	596.7	51.5	8741	299	2639
77	275.4	40.3	2623	12	3336
78	1023.3	52.4	8928	816	9392
79	404.2	59.7	3704	442	3597
80	93.8	48.5	542	36	376
81	163.5	73.3	534	164	1366
82	1398	62.6	6316	1408	15463
83	314.7	55.6	3722	141	1979
84	123.5	34.2	1365	4	828
85	551.8	49.5	4846	335	2798
86	388.8	32.5	5615	7	2605
87	564.6	40	6756	103	2275
88	1.2	58.9	14	0	11
89	1190.6	55.6	7910	463	18147
90	489.7	65.1	3051	472	4521
91	634.5	40.4	5931	143	2033
92	293.6	54.7	3685	215	233
93	814.7	67.1	3245	915	6251
94	407.7	38.4	6199	48	5144
95	448.8	59.3	2304	301	2699
96	484.7	35.2	11246	123	2632
97	142.4	43.8	1735	27	915
98	317.7	47.5	2468	87	6240
99	488.3	62.1	4068	354	5290
100	219.5	48.7	1717	80	2722
101	375.6	61	4213	207	2548
102	627.4	47.2	3638	141	8215
103	185.9	44.6	1712	23	2889
105	103.5	54.8	913	61	701
106	90.2	59	339	19	1367
107	604.3	51	2368	221	12431
108	947.3	55	5377	183	18362
109	589.4	46.3	2149	195	6186

Table S.7 (continued):

			No. Possible NBS Features		
Subcatchment No.	**Area (AC)**	**Impervious Cover (%)**	**BIOR**	**PMPV**	**TRBX**
111	339.2	68.4	1326	371	2715
112	236.7	61.1	621	115	7151
113	45.8	72.1	72	68	339
114	518.8	53.8	2244	150	12494
116	278.7	47.1	1650	42	3050
117	11.1	44.5	18	0	26
118	350.3	55.5	1165	186	4659
119	413.9	38.5	6706	26	4730
120	150.9	64.9	572	207	2181
121	264.1	43.1	1289	101	1848
123	144.6	56	528	98	984
124	383.9	56.2	2068	186	3162
125	252.5	60.8	637	141	4223
126	10.6	47.9	7	0	0
127	24.6	72.9	50	52	57
128	489	48.5	1604	91	2793
129	258	59	403	159	2750
130	367.1	58.1	1306	232	2556
131	6.4	53.2	11	0	119
132	284.7	60.3	765	233	3487
133	314.7	60.6	532	155	3444
134	296.5	63.3	1974	206	1981
135	484.7	51.3	1866	255	4755
136	335.2	80.9	486	687	3635
137	1051.4	63.4	2509	880	16024
138	753.6	56.7	2267	471	10215
139	448.8	80.6	617	921	3912
140	721.4	57.3	2162	329	11066
141	291.7	59.4	1007	126	2480
143	263.4	64.1	824	212	4076
144	747.2	68.3	345	698	23024
145	725.4	60.9	1298	395	15412
146	247.3	47.2	1255	23	5297
147	38.5	43	307	6	478
148	411.3	65.1	81	110	16841
149	147.6	68.7	107	96	4682

Table S.7 (continued):

			No. Possible NBS Features		
Subcatchment No.	**Area (AC)**	**Impervious Cover (%)**	**BIOR**	**PMPV**	**TRBX**
151	392.6	65.1	154	61	17508
152	379.4	55.9	916	171	9809
153	10.9	33.6	114	0	225
154	540.7	68.2	1114	314	10807
155	820.9	64.3	3071	998	12983
156	593.4	60.4	223	37	23936
157	94.3	56.3	596	13	2427
158	218	56.1	874	23	8214
159	177.2	55.1	982	62	4267
160	660.5	64.6	2867	750	13880
161	483.1	69	1038	559	8147
162	486.4	70.5	590	395	11047

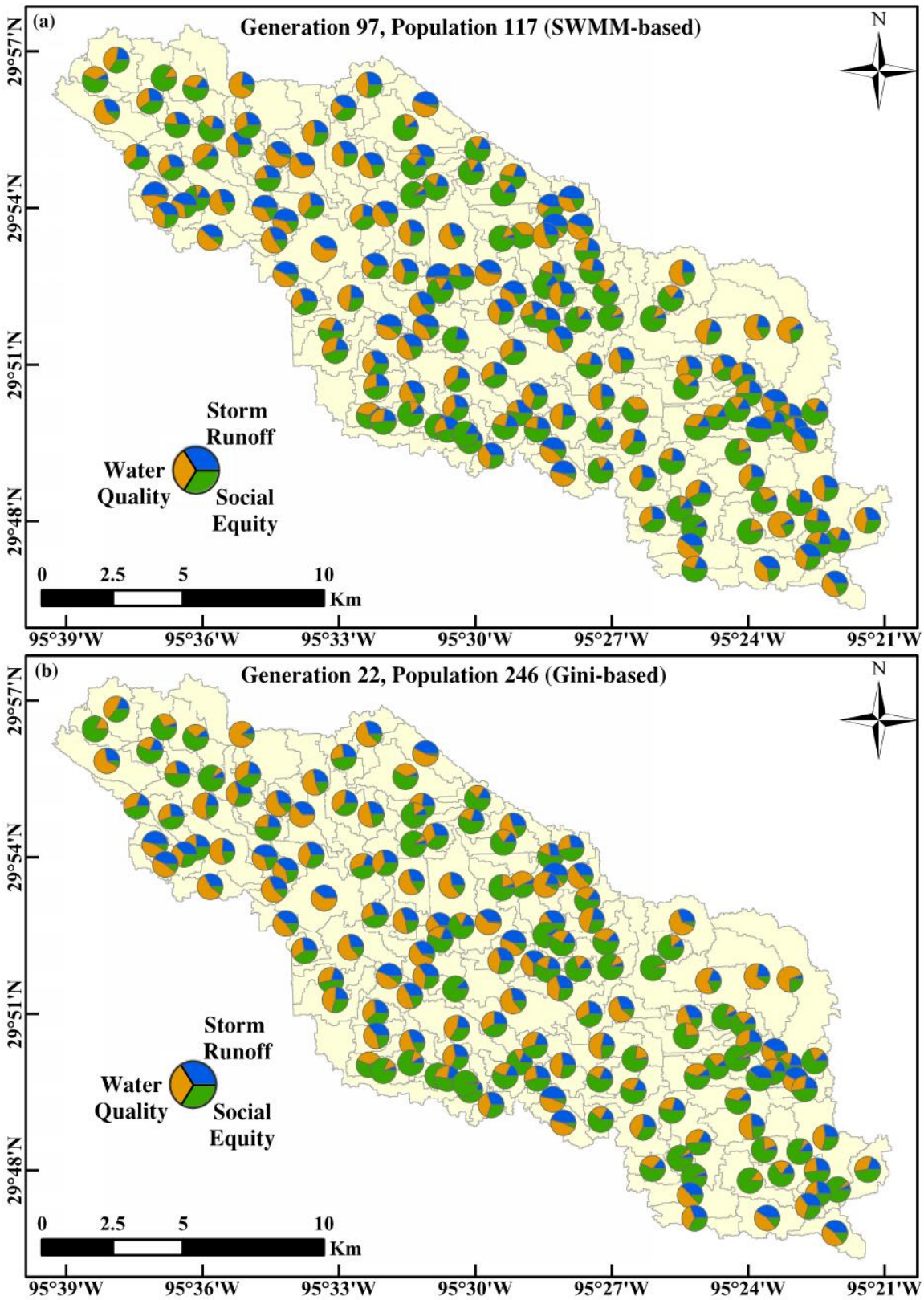

Figure S.4. Proportional representation of evaluation indicator efficiency for **(a)** SWMM-based optimization model, and **(b)** Gini-based optimization model.